mathematics

MDPI

Article

A Multi-Age Multi-Group Epidemiological Model and Its Validation on the COVID-19 Epidemic in Italy: SEIHRDV

Luca Dede' [1,*], Nicola Parolini [1], Alfio Quarteroni [1,2], Giulia Villani [3] and Giovanni Ziarelli [4]

[1] MOX, Department of Mathematics, Politecnico di Milano, 20133 Milan, Italy; nicola.parolini@polimi.it (N.P.); alfio.quarteroni@polimi.it (A.Q.)
[2] Institute of Mathematics, École Polytechnique Fédérale de Lausanne, 1015 Lausanne, Switzerland
[3] Department of Mathematics, University of Rome "La Sapienza", 00185 Rome, Italy; g.villani@uniroma1.it
[4] Department of Mathematics, Università degli Studi di Milano, 20133 Milan, Italy; giovanni.ziarelli@unimi.it
* Correspondence: luca.dede@polimi.it

Abstract: We propose a novel epidemiological model, referred to as SEIHRDV, for the numerical simulation of the COVID-19 epidemic, validated using data from Italy starting in September 2020. SEIHRDV includes the following compartments: Susceptible (S), Exposed (E), Infectious (I), Healing (H), Recovered (R), Deceased (D), and Vaccinated (V). The model is age-stratified, with the population divided into 15 age groups, and it considers seven different contexts of exposure to infection (family, home, school, work, transport, leisure, and other contexts), which impact the transmission mechanism. The primary goal of this work is to provide a valuable tool for analyzing the spread of the epidemic in Italy during 2020 and 2021, supporting the country's decision making processes. By leveraging the SEIHRDV model, we analyzed epidemic trends, assessed the efficacy of non-pharmaceutical interventions, and evaluated vaccination strategies, including the introduction of the Green Pass, a containment measure implemented in Italy in 2021. The model proved instrumental in conducting comprehensive what-if studies and scenario analyses tailored to Italy and its regions. Furthermore, SEIHRDV facilitated accurate forecasting of the future potential trajectory of the epidemic, providing critical insights for improved public health strategies and informed decision making for authorities.

Keywords: epidemiological model; numerical simulation; validation on COVID-19 epidemic

MSC: 92D30

check for updates

Academic Editor: Cristian Lazureanu

Received: 4 January 2025
Revised: 17 February 2025
Accepted: 26 February 2025
Published: 27 February 2025

Citation: Dede', L.; Parolini, N.; Quarteroni, A.; Villani, G.; Ziarelli, G. A Multi-Age Multi-Group Epidemiological Model and Its Validation on the COVID-19 Epidemic in Italy: SEIHRDV. *Mathematics* **2025**, *13*, 788. https://doi.org/10.3390/math13050788

Copyright: © 2025 by the authors. Licensee MDPI, Basel, Switzerland. This article is an open access article distributed under the terms and conditions of the Creative Commons Attribution (CC BY) license (https://creativecommons.org/licenses/by/4.0/).

1. Introduction

The coronavirus pandemic is a public health emergency that has affected the whole world since its outbreak in December 2019. Up to 6 December 2023, more than 6.9 million deaths had been registered, and more than 770 million cases had been detected according to the World Health Organization. In this context, various mathematical models have been proposed to describe the course of the epidemic and forecast its progression, aiming to assist authorities in selecting optimal control strategies to mitigate the spread of the virus. The primary objective is to prevent the collapse of the healthcare system and ultimately enhance the public health response [1].

Most epidemiological models are derived from the compartmental framework originally proposed by Kermack and McKendrick [2], known as the classic SIR model, which partitions the population into susceptible, infected, and recovered individuals; see also [3]. In recent years, numerous compartmental epidemiological models specifically designed

to describe the COVID-19 pandemic have been proposed. Generally, these models divide the population into subsets, called compartments, that represent different stages of disease progression. The associated mathematical formulations are often deterministic systems of Ordinary Differential Equations (ODEs) governing the mobility of individuals among compartments. The proposed models focus on different aspects that characterize the evolution of the epidemic. Some models incorporate spatial dynamics [4] (including network structures [5,6]), as well as social [7] and age [8] stratification, in order to cope with the effects of heterogeneity in the population. Other models proposed strategies for the calibration of time-dependent model parameters to account for the continuous changes in conditions, with respect to both virus behavior (through mutations and vaccine response, see, e.g., [9,10]) and social environment (through policy rules and non-pharmaceutical interventions as, for example, [11–13]). In addition, uncertainty in parameters can be incorporated by reformulating the problem as a set of stochastic differential equations [14,15]. Beyond compartmental models, various data-driven approaches have emerged, including agent-based models [16,17] and stochastic methods [18]. Among these approaches, machine learning algorithms are increasingly used, offering complementary perspectives for studying the dynamics of infectious diseases. Notable examples include physics-informed neural networks [19], disease-informed neural networks [20], structure-preserving neural networks [21], deep learning algorithms [22], operator learning methods [23], and model learning frameworks [24].

Building on the foundation of compartmental epidemiological models, the standard SIR model can be generalized to incorporate specific features of the disease under investigation, such as its virological and medical characteristics. Most of these models operate under the assumption of a homogeneous epidemic, disregarding distinctions in factors such as age groups, exposure contexts, and geographical variations that can influence transmission dynamics [25]. Although this simplification may reduce the accuracy of forecasts, homogeneous models are computationally efficient, straightforward to calibrate, and often yield results that are interpretive and actionable for policy making. Since the beginning of the pandemic, we have observed that the impact of COVID-19 infection varies with the age of infected individuals, with clear evidence showing that older people experience more severe outcomes than younger individuals. Additionally, the risk of infection varies depending on the context in which susceptible individuals come into contact with infected persons. Vaccinations, which were widely administered starting in 2021, have significantly impacted the transmission mechanisms of the virus and reduced the severity of symptoms, thereby mitigating the effects of COVID-19 [26].

In this work, we introduce a novel, age-stratified ODE-based compartmental model, named SEIHRDV, specifically designed to analyze the spread of COVID-19 in Italy from September 2020 to July 2021. Our model and analysis were carefully crafted to align with the specific context, situation, and data provided by Italian authorities during this period. Rather than focusing solely on individual health outcomes, the model's primary objective was to predict epidemic spread and dynamics, and support Italian authorities in decision making, particularly regarding non-pharmaceutical interventions (NPIs) targeting different exposure contexts and age groups [27]. It was applied to account for varying exposure contexts where infection occurred with differing probabilities, as well as the effects of the vaccination campaign (see, e.g., [28]).

The model leverages on *tables of contacts*, also known as Mossong tables [29], which detail the average daily number of contacts among members of different age groups across various exposure contexts. We consider the following contexts: home, school, work, transport, leisure, and others. As a key innovation, we refined the original *home* category in the Mossong tables by distinguishing between intra-household contacts (*family*) and

household-visitor contacts (*home*). This distinction is significant in capturing the impact of NPIs that imposed specific restrictions on interactions between relatives and friends visiting different households, as was the case in Italy during certain periods of the years 2020 and 2021 [30,31]. This enhanced model enables detailed evaluations of the effects of various NPIs with different levels of restrictions on social behaviors between 15 age groups and seven exposure contexts, supporting both retrospective analyses and future scenario projections.

Moreover, in this paper, we retrospectively assess the effectiveness of restrictions associated with the introduction of the Green Pass, an NPI implemented in Italy in 2021 to maximize vaccination coverage, particularly in public exposure contexts. By incorporating the Green Pass into the model, our objective was to simulate a realistic scenario, evaluate its efficacy in reducing infection rates in different contexts, and analyze its impact on the health outcomes of vaccinated individuals, extending our analysis to cover Italy until fall 2021.

We believe that our model offers valuable insights into the epidemic's spread, particularly through its ability to simulate and predict the outcomes of different NPIs. It was designed with the specific goal of supporting policymakers and authorities in Italy during 2020 and 2021, helping them to understand the implications of various interventions, and improving preparedness for future outbreaks. The model structure, which accounts for both age-stratified data and different exposure contexts, provides a more nuanced understanding of the virus's spread compared to homogeneous models. We present a detailed evaluation of the effectiveness of the Green Pass and other restrictions imposed during this period, making this work a critical tool for assessing past and future epidemic scenarios.

The paper is organized as follows: in Section 2, we describe the multi-age/multi-context structure of the mathematical model, introducing the different parameters and the way we derived the tables of contacts. Then, we describe the calibration process and how we take into account the vaccination campaign and the introduction of Green Pass restrictions. In Section 3, we show an extensive campaign of numerical results, set in Italy and two Italian administrative regions: Lombardy and Lazio. In Section 4, we draw our conclusions and discuss possible improvements and possible future extensions of the SEIHRDV model.

2. Mathematical Model

Starting from the standard SEIR model [32], we developed an ODE-based compartmental model tailored to COVID-19. In Section 2.1, we present the homogeneous SEIHRDV model as a foundational framework. In Section 2.2, we extend this model to incorporate multi-age and multi-context dynamics. Section 2.3 details the implementation of these multi-age and multi-context elements. Finally, in Section 2.4, we outline the calibration procedure, including the integration of vaccination data and considerations related to the Green Pass policy.

2.1. SEIHRDV Model

When a *Susceptible* individual (compartment S) is infected but still in the incubation period, a transition to the *Exposed* state (compartment E) occurs. After the incubation period, an Exposed individual becomes *Infected* (compartment I) and can transmit the infection. Before recovery, infected individuals enter the *Healing* state (compartment H), during which they remain positive but are no longer infectious; H includes infected individuals, whether recovering at home, in quarantine, or in a hospital. The progression of the disease ultimately results in either full recovery (*Recovered*, compartment R) or death (*Dead*, compartment D). To account for the vaccination campaign, we introduce a *Vaccinated* compartment (V), which accounts for individuals who have received at least the first dose of the vaccine.

In this work, we neglect the effects of second-dose vaccinations, as our analysis concludes in the summer of 2021, while widespread second-dose administration in Italy only began in September 2021. A possible extension of the model, which incorporates the complete vaccination cycle, could be inspired by [33].

The SEIHRDV model (see Figure 1) is designed to describe all the stages an individual may undergo, from being susceptible to entering the healing phase. The corresponding mathematical model is given by the following:

$$
\begin{aligned}
&\frac{dS}{dt} = -c\,\beta\,\frac{S\,I}{N} - \rho\,\frac{S}{S+R} + \mu_R\,R + \mu_V\,V,\\
&\frac{dE}{dt} = c\,\beta\frac{(S+\sigma V)\,I}{N} - \alpha E,\\
&\frac{dI}{dt} = \alpha\,E - \gamma\,I,\\
&\frac{dH}{dt} = \gamma\,I - \omega\,H \qquad\qquad t \in (0,T],\\
&\frac{dR}{dt} = (1-f(S,V))\,\omega\,H - \mu_R\,R,\\
&\frac{dD}{dt} = f(S,V)\,\omega\,H,\\
&\frac{dV}{dt} = -\sigma\,c\,\beta\,\frac{V\,I}{N} + \rho\,\frac{S}{S+R} - \mu_V\,V,\\
&S(0) = S_0, \quad E(0) = E_0, \quad I(0) = I_0, \quad H(0) = H_0,\\
&R(0) = R_0, \quad D(0) = D_0, \quad V(0) = V_0
\end{aligned}
\tag{1}
$$

where N denotes the total number of individuals of the population, which is given by the sum of the number of individuals belonging to one of the 7 compartments, namely $N = S + E + I + H + R + D + V$. Albeit each compartment changes in time, we assume that the total number of individuals N in the population remains constant over time.

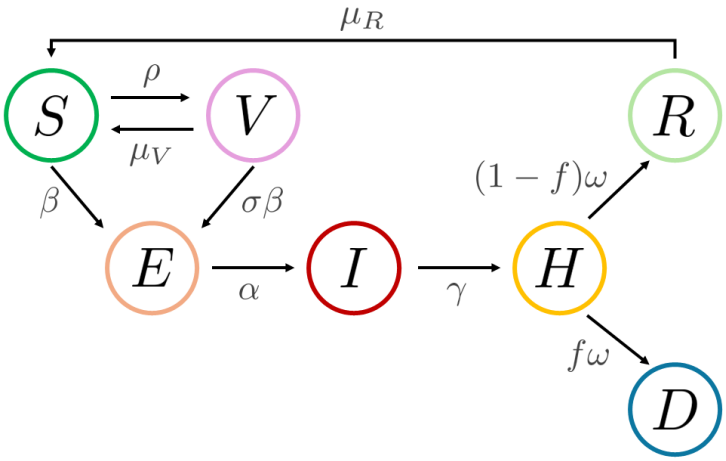


Figure 1. Sketch of SEIHRDV model (S = Susceptible, E = Exposed, I = Infectious, H = Healing, R = Recovered, D = Deceased, V = Vaccinated).

The SEIHRDV model is characterized by the following parameters:

- the product $(c\,\beta)$ stands as the transmission rate due to contacts between a susceptible individual and an infected individual, where $\beta : (0,T] \to \mathbb{R}$ is a time-dependent function that captures the variation in contacts, which also depends on the implementation of possible NPIs, while $c : (0,T] \to \mathbb{R}$ embodies changes in the transmission rate, which we will extract from data during the calibration process (cf. Section 2.4.1);

- $\alpha > 0$ denotes the rate at which an exposed individual becomes infectious and is defined as the inverse of the average incubation time;
- $\gamma > 0$ denotes the rate at which an infectious individual becomes unable to infect, but is still infected. This rate is derived from the average infectious time;
- $\omega > 0$ is a rate derived from the average removal time for the deceased, and it is multiplied by f or $1 - f$;
- $\sigma \in [0, 1]$ denotes the inefficacy rate of the vaccine in the transmissibility of the disease [34];
- $f : [\tau, T] \to [0, 1]$ is the fatality function, defined as

$$f(t) = f(S(t), V(t); \tau) = \hat{f}\, \frac{S(t-\tau) + \theta\, \sigma\, V(t-\tau)}{S(t-\tau) + \sigma\, V(t-\tau)}, \tag{2}$$

  where $\hat{f}$ is the *infectious fatality rate* ([35]) taken from an Imperial College report of October 2020 [36], and τ is the average elapsing time between the first exposition and death, that we set at 25 days according to clinical studies [37]. We introduce the parameter $\theta \in [0, 1]$, which denotes the rate of inefficacy of the vaccine in reducing the severity of the disease. In this way, f is obtained by rescaling the original $\hat{f}$ with the ratio between the sum of individuals Susceptible and Vaccinated, in which the vaccine is not effective either in reducing the transmissibility of the virus or in reducing the severity of the disease, and all the individuals who can potentially contract the virus;
- $\rho \in \mathbb{N}$ represents the number of the average of first doses administered daily (doses per day), estimated from the data made available from Dipartimento di Protezione Civile Italiana https://github.com/italia/covid19-opendata-vaccini (accessed on 1 March 2021);
- $\mu_R > 0$ and $\mu_V > 0$ denote the waning immunity rates for Recovered and Vaccinated individuals respectively, i.e., the rate at which Recovered individuals and Vaccinated individuals, respectively, come back to the susceptible compartment.

In our model, the parameters α, γ, ω, θ, $\hat{f}$, μ_R, and μ_V are kept fixed in time, while $\rho = \rho(t)$, $\beta = \beta(t)$, and $\sigma = \sigma(t)$ are instead functions of time. The values of these parameters have been deduced from established studies [26] or directly from available data. Following the methodology in [10], we estimate the initialization of compartments that are not directly accessible from the data provided by the Dipartimento di Protezione Civile Italiana https://github.com/pcm-dpc/COVID-19 (accessed on 1 March 2021), such as the Exposed and Infected individuals. This estimation is obtained thanks to algebraic relationships among measurable quantities, including the CFR (Case Fatality Rate), IFR (Infection Fatality Rate) [36], and the recorded number of deceased individuals. The number of delivered doses ρ in (1) is rescaled by the factor $\frac{S}{S+R}$ to take into account that a portion of doses are administered to both detected and undetected recovered individuals.

2.2. The Multi-Age and Multi-Context SEIHRDV Model

In this section, we present the SEIHRDV model. We consider the following:

- $N_a = 15$ age groups, by assigning to each of the following age groups the corresponding SEIHRDV variables: {0–4, 5–9, 10–14, 15–19, 20–24, 25–29, 30–34, 35–39, 40–44, 45–49, 50–54, 55–59, 60–64, 65–69, 70+};
- $K = 7$ contexts of exposition: family, home, school, work, transport, leisure, and other.

The interactions among the compartments of the various age groups ([38]) in the different exposure contexts are sketched in Figure 2. For the sake of simplicity, we limited ourselves to two age groups, named *group 1* and *group 2*, and only one exposure context for each age group. The corresponding compartments are denoted with S_i, E_i, I_i, H_i, R_i,

D_i, and V_i, with $i \in 1, 2$. The disease spreads when an individual from S_1 is in contact with either an infectious individual from the same age group, I_1, or an individual from I_2. Therefore, the transmission rate β of the virus is replaced by the expression $\frac{\beta_{11} I_1 + \beta_{12} I_2}{I_1}$, which takes into account both possible contacts. The same holds for an individual in S_2 with the appropriate modifications.

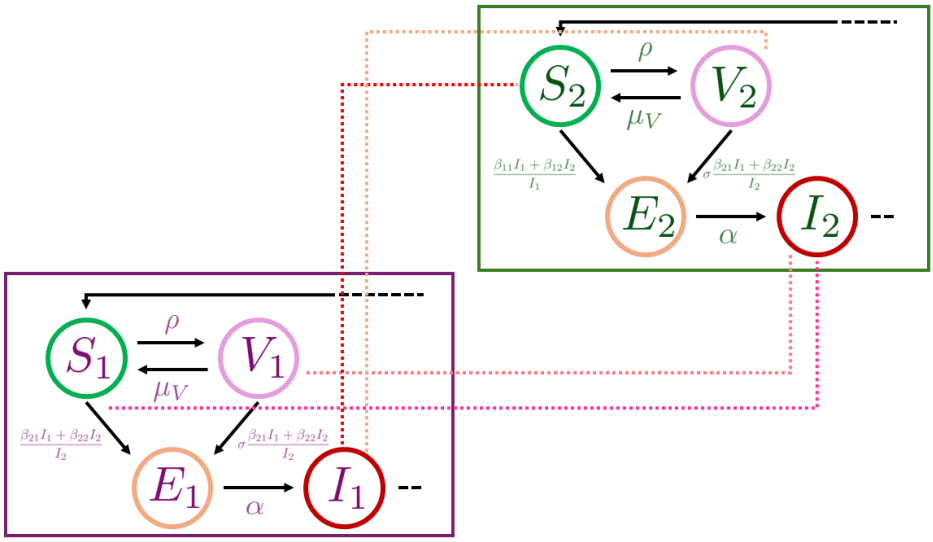


Figure 2. Sketch of the SEIHRV model in a single exposure context and two ages group.

By extending this argument for all the $N_a = 15$ age groups, and considering the $K = 7$ contexts of exposition, we obtained the complete SEIHRDV multi-age and multi-group model (Figure 3): an individual of age group i can have contact with infectious individuals belonging to the N_a age groups in the K contexts of exposition. In particular, we denote by E_i^k the number of individuals in the age group i who become exposed in the context k, and by β_{ij}^k the transmission rate of I_j in contact with S_i in the context of exposition k. In the multi-age and multi-context SEIHRDV, β can be seen as a third order tensor with components β_{ij}^k.

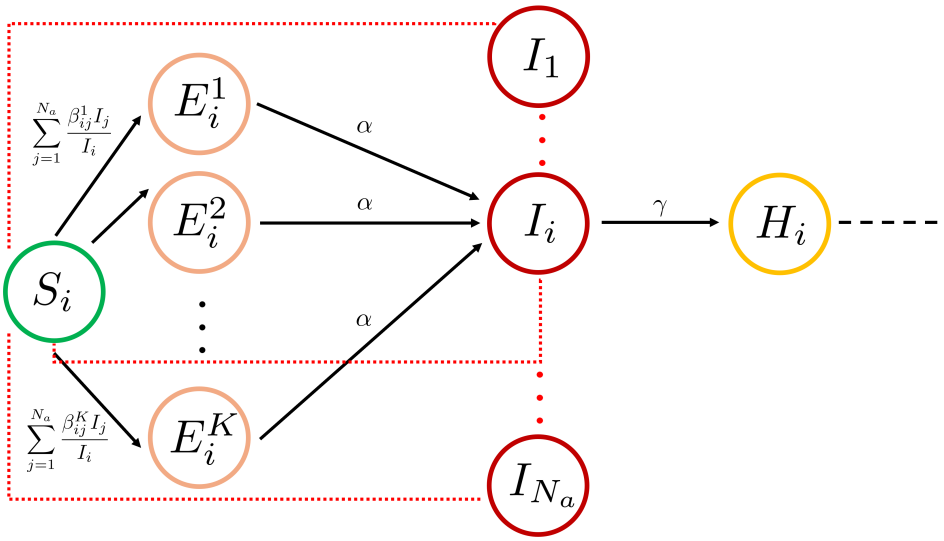


Figure 3. Interactions among the compartments in the SEIHRDV multi-age and multi-group model, with $K = 7$ contexts of exposition and $N_a = 15$ age groups.

The equations describing the multi-age and multi-context model read as follows:

$$
\begin{aligned}
&\frac{dS_i}{dt} = -\left(\sum_{k=1}^{K}\left(\sum_{j=1}^{N_a} c\,\beta_{ij}^{k} I_j\right)\right)\frac{S_i}{N_i} - \rho_i\,\frac{S_i}{S_i+R_i} + \mu_R\,R_i + \mu_V\,V_i,\\
&\frac{dE_i^k}{dt} = \left(\sum_{j=1}^{N_a} c\,\beta_{ij}^{k} I_j\right)\frac{(S_i+\sigma\,V_i)}{N_i} - \alpha\,E_i^k, \qquad k=1,\ldots,K,\\
&\frac{dI_i}{dt} = \alpha\left(\sum_{k=1}^{K} E_i^k\right) - \gamma I_i,\\
&\frac{dH_i}{dt} = \gamma I_i - \omega H_i, \qquad t\in(0,T]\\
&\frac{dR_i}{dt} = (1-f(S_i,V_i))\,\omega\,H_i - \mu_R R_i, \qquad (3)\\
&\frac{dD_i}{dt} = f(S_i,V_i)\,\omega\,H_i,\\
&\frac{dV_i}{dt} = -\left(\sum_{k=1}^{K}\left(\sum_{j=1}^{N_a} c\beta_{ij}^{k} I_j\right)\right)\frac{\sigma V_i}{N_i} + \rho_i\,\frac{S_i}{S_i+R_i} - \mu_V V_i,\\
&S_i(0)=S_{i_0}, \quad E_i^k(0)=E_{i_0}^k, \quad I_i(0)=I_{i_0}, \quad H_i(0)=H_{i_0},\\
&\qquad\qquad R_i(0)=R_{i_0}, \quad D_i(0)=D_{i_0}, \quad V_i(0)=V_{i_0},
\end{aligned}
$$

$\forall\ i=1,\ldots,N_a.$

2.3. Tables of Contacts and β-Matrices

To estimate the transmissibility rate β for different age groups in different exposure contexts, we used the tables of contacts, based on those proposed by the POLYMOD study [29]. The social contact matrices reported in [29] for different countries estimate the average number of contacts that individuals from an age group have in the following contexts: home, school, work, transport, leisure, and other. In particular, we used the table referring to the Italian case that was also considered by the Italian Scientific Technical Committee (CTS) in the early phase of the COVID-19 epidemic (see [39]). The CTS was established in Italy in February 2020 to provide advice and support for coordination activities to overcome the epidemiological emergency due to the spread of the coronavirus; see also [40]. More recent contact matrices were not used because our study was designed to align with the official data and methodologies adopted by Italian authorities during the 2020–2021 period. We believe that alternative contact tables could have introduced inconsistencies with these reference studies, potentially compromising the comparability and interpretability of our findings within the framework of Italian public health analyses.

In addition to the 5 exposure contexts outside the household, as outlined in [29], we accounted for a total of $K = 7$ distinct exposure contexts. Specifically, based on data from the Italian National Statistics Institute (ISTAT) regarding population and household composition, we disaggregated household contacts into two categories: those occurring exclusively among family members (*"family"*) and those involving both family and non-family members (*"home"*). This distinction enables the consideration of different restrictions implemented in Italy during short periods in 2021. Notably, in specific administrative regions, visits to family members were occasionally prohibited. The actual social contact matrix used in the present work is reported in Table 1.

Table 1. Average number of contacts by age groups, total and disaggregated, by social context in which the contact takes place, adding "family" context.

		Exposure Context						
Ages	**Tot**	**Family**	**Home**	**School**	**Work**	**Transport**	**Leisure**	**Other**
0–4	16.54	2.30	2.19	5.27	0.00	0.98	3.06	2.75
5–9	20.49	2.27	2.34	8.87	0.00	1.12	4.53	1.37
10–14	27.38	2.21	2.22	11.98	0.20	1.35	5.62	3.80
15–19	29.28	2.05	2.54	13.22	0.05	1.74	6.83	2.87
20–24	22.15	1.49	2.02	1.17	4.49	0.96	7.23	4.80
25–29	21.00	1.04	2.43	2.23	5.21	1.13	6.30	2.66
30–34	18.03	1.26	2.29	0.85	3.92	0.76	5.24	3.72
35–39	21.25	1.75	2.63	0.68	7.78	1.05	3.92	3.45
40–44	22.35	1.63	2.25	2.53	7.00	0.67	4.48	3.79
45–49	19.27	1.50	1.49	2.61	8.24	0.88	1.93	2.64
50–54	22.30	1.38	1.37	5.54	8.05	0.52	2.02	3.41
55–59	18.27	1.11	1.77	1.41	4.60	0.68	3.62	5.06
60–64	18.43	0.91	2.37	1.07	6.05	0.87	3.53	3.63
65–69	12.74	0.71	2.39	0.55	0.48	0.95	3.33	4.33
70+	10.55	0.71	2.53	0.06	1.04	0.22	4.22	1.77

On the basis of the social contact data provided in [29], it is possible to estimate, for each context of exposition, the daily contacts of each individual distributed in the different age groups (cf. Figure 4), as well as the total number of daily contacts that each individual of a given age group has with individuals in different age groups and in different contexts of exposition (cf. Figure 5).

These contact matrices have been used to determine the $\beta - matrices$ that express the transmissibility rate for each age class in each exposure context. However, the number of contacts is not the only factor that should be taken into account. Indeed, as suggested in [39], age-dependent susceptibility to the infection should also be considered, which we denote $risk_A$ (Table 2), as well as different levels of risk to contract the virus in the different contexts of exposition [41], denoted as $risk_E$ (Table 3).

Table 2. Susceptibility by age group.

Age Groups	0–4	5–9	10–14	15–19	20–24	25–29	30–34	35–39
$\mathbf{risk_A}$	0.34	0.34	0.34	1	1	1	1	1
Age Groups	40–44	45–49	50–54	55–59	60–64	65–69	70+	
$\mathbf{risk_A}$	1	1	1	1	1	1.47	1.47	

Table 3. Levels of risk associated with the contexts of exposition.

Level of Risk	Low	Medium–Low	Medium	Medium–High	High	Very High
$\mathbf{risk_E}$	0.25	0.5	1	1.5	2	2.5

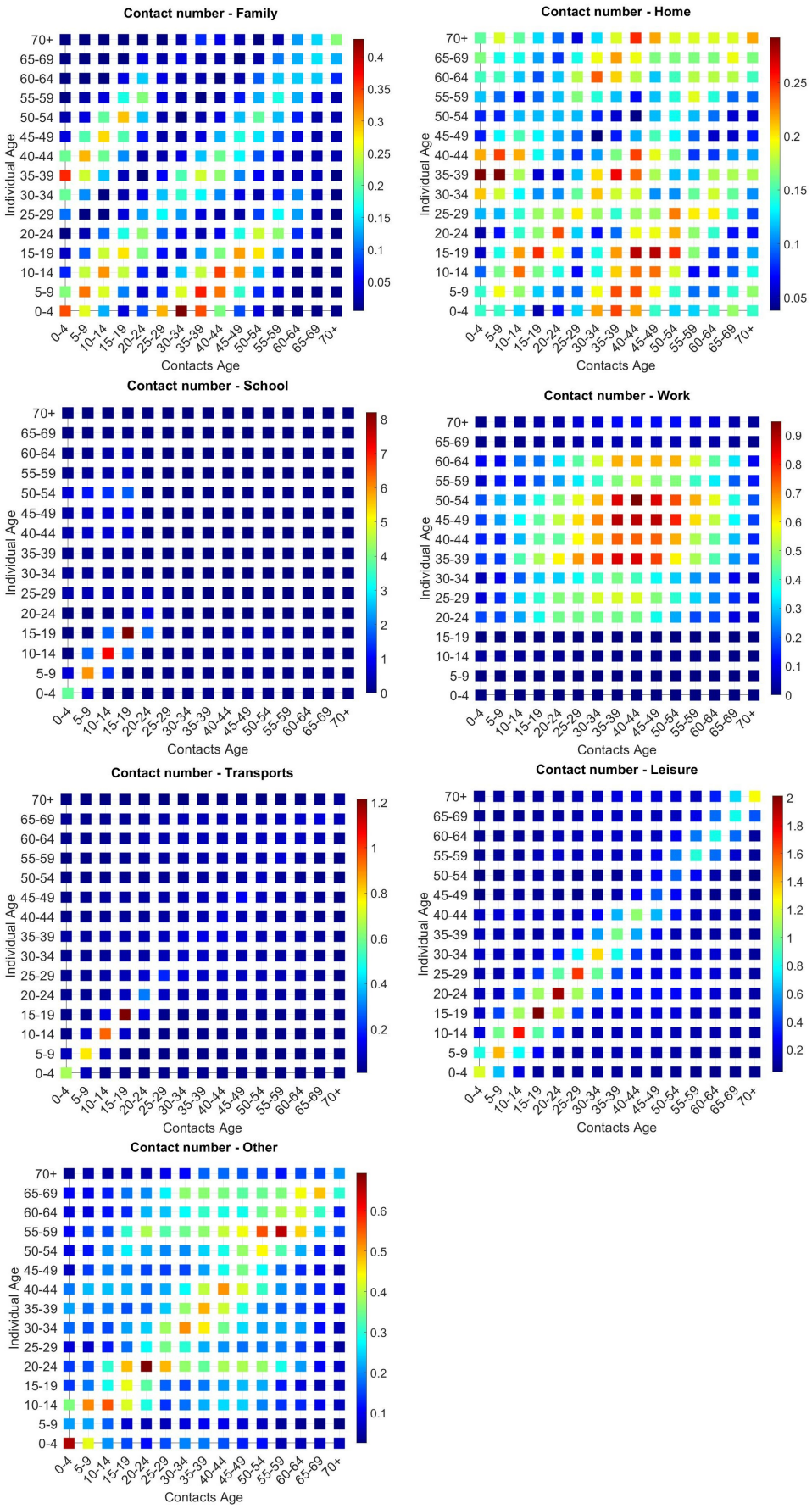


Figure 4. POLYMOD matrices $M^k_{i,j}$, $k = 1, \ldots, 7 = K$, $i, j = 1, \ldots, 15 = N_a$: total number of contacts that each individual has with individuals from the 15 age groups, in the seven contexts of exposition.

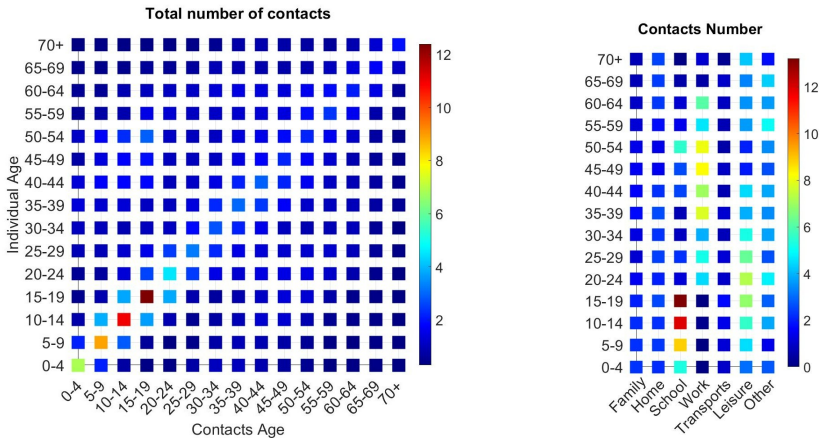


Figure 5. Total number of contacts that each individual has with individuals from the 15 age groups on the left, for each exposure context on the right.

The risk associated with each age group is based on a CTS report [39], which states that children under 14 have a 66% lower-than-average risk of contracting infection, while adults over the age of 65 have a 47% above average risk of infection. On the other hand, the risk factor associated with each exposure context depends on the relative contribution of the various sectors (sub-contexts) that constitute it. Specifically, we assigned a risk level to each sector by considering four key factors: the presence of closed spaces, the duration of interactions, the density of the crowd, and activities involving forced exhalation (such as sneezing, yelling, singing, and coughing). For the following contexts of exposition, we considered different sectors as follow:

- **school context**: split into six sectors (nursery, kindergarten, elementary school, middle school, high school, and university);
- **work context**: divided into seven sectors (essential, healthcare, manufacturing, trade, construction, restaurant/hotel, other);
- **leisure context**: divided into six sectors (outdoor restaurants, indoor restaurants, outdoor pub/disco, indoor pub/disco, indoor sport, outdoor sport);
- **"other" context**: divided into three sectors (essential retail, other non-essential retail, and mass and religious events).

The home context takes into account contacts that occur in households, but not among co-habitants, which are instead referred to in the family context. No split was considered for the transport context.

Then, a scenario can be defined by assigning values in $[0,1]$ for each sector of the various contexts to indicate their opening/closing, considered according to the regulations in force (0 if the sector is totally closed, 1 if it is totally open, values in $(0,1)$ if there are other restrictions). To obtain the $\beta - matrix$ that expresses the effective risk of transmission for each age group in contact with other age groups in the different contexts of exposition, we multiplied the k-th contact matrix by a function depending on the risk parameters defined above and on the chosen scenario, which expresses the level of opening/closure of the sub-contexts:

$$\beta_{i,j}^{k} = M_{i,j}^{k}\, h_k(risk_E^{S_k}, risk_A, scenario_k^{l}) \quad \text{for all } l = 1,\ldots,S_k, \quad \text{for all } k = 1,\ldots,K, \quad (4)$$

where i is the age of the individual, j is the age of the contact, M^k is the contact matrix of the context k, S_k is the number of sectors of the kth context of exposition, and h_k is a piece-wise constant context-dependent function, in which we calculate a value expressing the global risk associated with the specific context k for each age group. The latter function depends on the following:

- $risk_E^{S_k}$, that is the value of risk assigned to each of the S_k sectors of the context k between low, medium–low, medium, medium–high, high, and very high risk (Table 3);
- $risk_{Ai}$, that is the vector containing the risk for each age group (Table 2);
- $scenario_k^l$, that is the level of opening/closing (in $[0, 1]$) of each sector l of the exposure context k, as we defined before.

Starting in November 2020, in Italy, containment measures differentiated by region were introduced due to the fact that the spread of the virus was different on the peninsula. This differentiation is expressed in colors: *yellow* for the regions with a transmissibility index lower than 1.25; *orange* for regions with transmissibility index between 1.25 and 1.5, where the associated NPIs have more restrictions; and *red* for regions with a transmissibility index greater than 1.5. The NPIs associated with red regions were the more restrictive, corresponding to almost complete lockdowns. These measures were issued with an order from the Minister of Health, in agreement with the president of the region concerned and the CTS, and had to have a minimum duration of 15 days, since their impact on the transmission mechanism is delayed, as estimated, e.g., in [42]. The conditions for the regions to switch the associated colors changed during the evolution of the pandemic, and *white* zones were also introduced in January 2021, corresponding to the almost complete dismissal of mobility restrictions.

In Figure 6, we can see the $\beta - matrices$ of the school context associated with two different scenarios: the yellow zone and the red zone. In the yellow zone, the restrictions included schools totally open up to the third year of middle school and high schools open to 50%, while in the red zone we have schools open up to the first year of middle school, while the second and third years of middle school, high schools, and universities were totally closed.

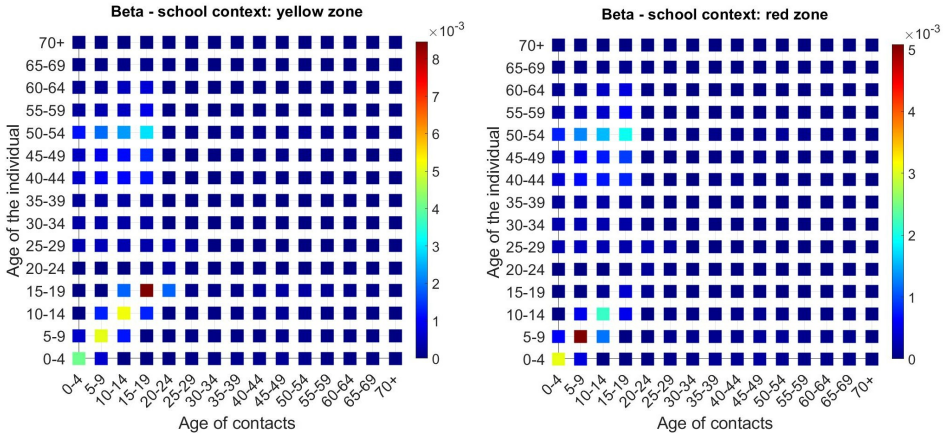


Figure 6. $\beta - matrices$ in the school context: yellow zone scenario on the left, red zone scenario on the right.

With different containment measures in force for each region, to define the scenario, we have to make different considerations depending on whether we are simulating on a national or regional basis. At the regional level, it is sufficient to reconstruct the temporal history of the regional restrictions, and at the national level it is instead necessary to take into account the different containment measures in force in each region, and to reconstruct an average measure for the restrictions. To do this, for each week, we analyzed the regional restrictions in force (which regions were in yellow zone, which in orange, which in red, which in white), and we set the final scenario weighing all these different scenarios on the population of each region. In fact, regions with small populations have less weight on the Italian situation than large regions.

In the national case, we considered an array **n** in which each component corresponds to the number of inhabitants of an Italian region. Moreover, we considered arrays for each color zone (for example red zone, orange zone, yellow zone, and green zone), having one entry for each region, in which we had 1 if the corresponding region (in the same order as the previous array) had a government restriction of that color, and 0 if there were other color restrictions. For example, calling **r** the array of binary values corresponding to red zone, **o** the respective array for the orange zone, **y** for the yellow zone, and **w** for the white one. Multiplying the inhabitants array **n** with each color zone array, we obtained the number of the Italian population under that color zone restriction:

$$r_n = \sum_{i=1}^{N} \mathbf{r}_i \mathbf{n}_i, \qquad o_n = \sum_{i=1}^{N} \mathbf{o}_i \mathbf{n}_i, \qquad y_n = \sum_{i=1}^{N} \mathbf{y}_i \mathbf{n}_i, \qquad \text{and} \qquad w_n = \sum_{i=1}^{N} \mathbf{w}_i \mathbf{n}_i,$$

where r_n is the number of Italian people in red zone restrictions, o_n is the number of Italian people in orange zone restrictions, y_n is the number of Italian people in yellow zone restrictions, and w_n is the number of Italian people in white zone restrictions.

Finally, we derived the national scenario by averaging as follows:

$$scenario_k^l = \frac{r_n s_{r_k}^l + o_n s_{o_k}^l + y_n s_{y_k}^l + w_n s_{w_k}^l}{r_n + o_n + y_n + w_n}, \qquad l \in 1, \ldots, S_k, \quad k \in 1, \ldots, K$$

where $scenario_k^l$ is the value in $[0, 1]$ assigned to the lth sector of the kth context of exposition of the scenario, $s_{r_k}^l$. Instead, $s_{o_k}^l$, $s_{y_k}^l$, and $s_{w_k}^l$ are the values in $[0, 1]$ assigned to the lth sector of the kth context of exposition of the red zone scenario, the orange zone scenario, the yellow zone scenario, and the white zone scenario, respectively.

2.4. Data Generation and Calibration of the Parameters

In this section, we describe the calibration procedure (see Section 2.4.1) for determining model parameters that could not be directly derived from clinical or population cohort studies. Furthermore, we detail the processing of vaccination data (cf. Section 2.4.2) and describe the adjustments made to the model to incorporate the social restrictions introduced under the *Green Pass* initiative (cf. Section 2.4.3).

2.4.1. Calibration

Model calibration poses significant challenges in epidemic modeling, as inaccurate reconstructions can critically compromise the quality of scenario analyses and forecasts. Special attention must be given to parameters governing the transmission mechanism, particularly the function $c(t)$ in our model, as it plays a pivotal role in determining the model's reliability [24].

For this purpose, we performed a least squares calibration procedure based on reported deceased data from Dipartimento di Protezione Civile Italiana (DPC). Indeed, the deceased compartment is the only one with a direct counterpart in the DPC data and is generally the least affected by monitoring uncertainties. In our cases, both $c(t)$ and $\beta(t)$ (cf. Section 2.1) are piece-wise constant functions. The values of $c(t) = \sum_{i}^{N_{int}} c_i I_{(t_i, t_{i+1}]}(t)$ are calibrated separately for each time subinterval corresponding to a specific scenario (e.g., a particular restriction level). The iterative calibration stage is carried out according to the following steps:

1. Associate a $\beta - matrix$ for each subinterval corresponding to the prescribed scenario;

2. Solve the following optimization problem:

$$\min_{\{c_i\}_i} J(c) = \sum_{t=0}^{T} \frac{(D(t) - \hat{D}(t))^2}{\left(\hat{D}(t)\right)^2}, \tag{5}$$

where $\hat{D}$ is the total number of deceased individuals provided by the DPC in $[0, T]$.

2.4.2. Vaccination Campaign

The Italian COVID-19 vaccination campaign included the administration of two doses and a booster (third) dose in the late periods of the outbreak. These dynamics are incorporated into our model using vaccination data provided by DPC, enabling us to track the participation of individuals in the vaccination campaign. At the beginning of the vaccination campaign, vaccinations were initially delivered by age group. In particular, the data provided by the authorities were split into eight age groups {0–9, 10–19, 20–29, 30–39, 40–49, 50–59, 60–69, 70+}, even though in our model we consider fifteen age groups {0–4, 5–9, 10–14, 15–19, 20–24, 25–29, 30–34, 35–39, 40–44, 45–49, 50–54, 55–59, 60–64, 65–69, 70+} for better capturing different exposure contexts (such as schools and workplaces) and to track positive cases across age groups, which can be highly heterogeneous. Since our model includes a finer division of age groups, we need to disaggregate the broader age group data to match our model's structure and set the initial conditions. To achieve this, we make the following assumption. Let us call A_i the age groups provided by data, with $i = 1, \ldots, 8$, and B_j the age groups used in our model, with $j = 1, \ldots, 15$; the number of the initial vaccinated individuals of the age groups B_j is given by

$$|B_j| = \frac{|A_k|}{2}, \quad j = 1, \ldots, 14,$$

where

$$k = \begin{cases} \left\lfloor j/2 \right\rfloor + 1 & \text{if} \quad j \mod 2 = 1 \\ \left\lfloor j/2 \right\rfloor & \text{if} \quad j \mod 2 = 0 \end{cases} \tag{6}$$

and $|B_{15}| = |A_8|$. In this way, we are able to exploit the SEIHRDV multi-age and multi-group for reproducing the curve of vaccinated people evolving over time for each age group. In Figure 7, we report this evolution in the eight DPC age classes, finding agreement with the actual administrations *per age*.

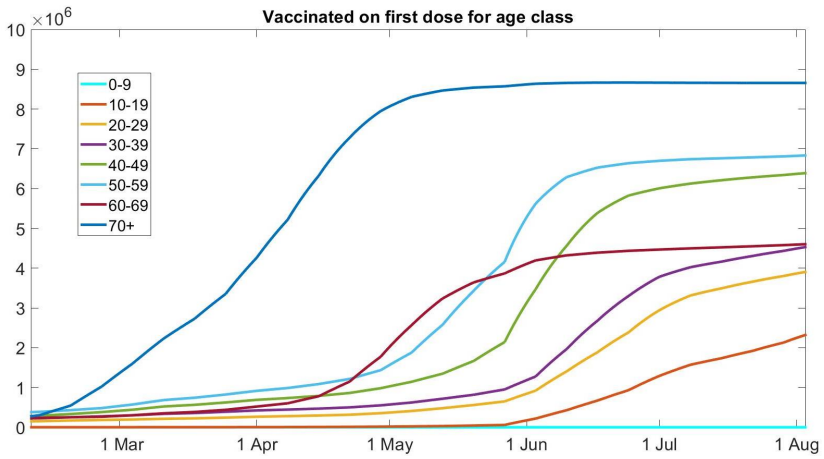


Figure 7. Vaccinated with first dose for DPC age groups.

In our model, we explicitly include only individuals vaccinated with at least one dose in the compartment V. The efficacy parameter σ, as estimated from clinical trials [26], was an appropriate choice when the number of individuals with only the first dose surpassed that of fully vaccinated individuals. However, by the end of 2021, approximately 78% of the Italian population had received at least one dose, with nearly 74% fully vaccinated. Furthermore, vaccine effectiveness in reducing COVID-19 transmissibility is estimated to decline approximately six months after full vaccination, necessitating the introduction of the third, or booster, dose. Consequently, for these later periods, we compute σ as a weighted parameter, determined as follows:

$$\sigma(t) = \frac{\sigma_1 V_{D_1}(t) + \sigma_2 \left(V_{D_2}(t) + V_{D_4}(t)\right) + \sigma_3 V_{D_3}(t)}{V_{D_1}(t) + V_{D_2}(t) + V_{D_3}(t) + V_{D_4}(t)}, \tag{7}$$

with

- σ_1, rate of ineffectiveness in reducing virus transmissibility for those who received only the first dose of the vaccine;
- σ_2, rate of ineffectiveness in reducing virus transmissibility for those who have been fully vaccinated (double dose of vaccine) for less than six months;
- σ_3, rate of ineffectiveness in reducing virus transmissibility for those who have been fully vaccinated (double dose of vaccine) for more than six months;
- $V_{D_1}(t)$ number of individuals who received only the first dose of vaccine on day t (DPC);
- $V_{D_2}(t)$ number of individuals who were fully vaccinated (with two doses) for less than six months on day t (DPC);
- $V_{D_3}(t)$ number of individuals who were fully vaccinated (with two doses) for more than six months on day t (DPC);
- $V_{D_4}(t)$ number of individuals who were vaccinated with the booster dose on day t (DPC).

We assume that the individuals receiving the booster dose regained the vaccine efficacy achieved in the first few months after full vaccination. In our model, we do not distinguish the various vaccines used; hence, the ineffectiveness values are estimated from average values from different vaccine data collected in the literature. In particular, we estimate $\sigma_1 = 0.30$, $\sigma_2 = 0.12$, and $\sigma_3 = 0.50$.

Finally, to determine the value of θ, introduced in the model in (2), we utilized data from the ISS as reported in [43]. Specifically, we analyzed the ratio of unvaccinated individuals who died relative to unvaccinated COVID-19 diagnoses and the ratio of vaccinated individuals who died relative to vaccinated COVID-19 diagnoses. From this analysis, we set $\theta = 0.8$, which implies that for vaccinated individuals diagnosed with COVID-19, the vaccine reduces mortality by 20%.

2.4.3. Green Pass

On 17 June 2021, Italy introduced the Green Pass restriction for the first time. The Green Pass, a digital COVID certificate proposed by the European Commission, aimed to facilitate the safe and unrestricted movement of European Union citizens during the COVID-19 pandemic. In Italy, the Green Pass certified one of the following conditions: receipt of a COVID-19 vaccination (issued after each vaccine dose), a negative result from a rapid antigen test within the previous 48 h or a molecular test within the previous 72 h, or recovery from COVID-19 within the previous 6 months.

We modified the model to take into account the restrictions due to the Green Pass (Figure 8).

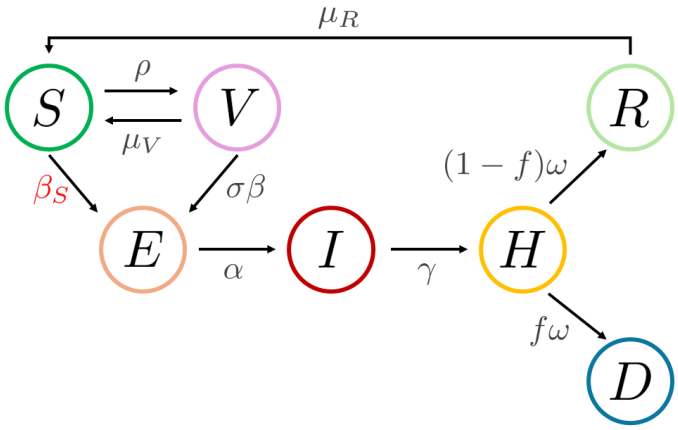


Figure 8. SEIHRDV model adapted to take into account Green Pass restrictions.

For this purpose, we introduced a second rate of transmissibility, β_S, which expresses the probability that a susceptible individual will contract the virus after a contact with an infectious individual, considering the limitations due to not having the Green Pass. For simplicity, we consider Green Pass holders as individuals who have received at least one dose of vaccine. Therefore, the individuals in V, who are Green Pass holders, are not subject to the same restrictions. For them, we consider the transmissibility rate β defined earlier. If the Green Pass restrictions were lifted, then $\beta_S = \beta$. Therefore, the equations become the following:

$$
\begin{aligned}
\frac{dS_i}{dt} &= -\left(\sum_{k=1}^{K}\left(\sum_{j=1}^{M} c(t)\,\beta_{S_{ij}^k} I_j\right)\right)\frac{S_i}{N_i} - \rho_i\,\frac{S_i}{S_i+R_i} + \mu_R\,R_i + \mu_V\,V_i,\\
\frac{dE_i^k}{dt} &= \left(\sum_{j=1}^{M} c(t)\,\beta_{S_{ij}^k} I_j\right)\frac{S_i}{N_i} + \left(\sum_{j=1}^{M} c(t)\,\beta_{ij}^k I_j\right)\frac{\sigma V_i}{N_i} - \alpha\,E_i^k, \qquad k=1,\dots,K,\\
\frac{dI_i}{dt} &= \alpha\left(\sum_{k=1}^{K} E_i^k\right) - \gamma\,I_i,\\
\frac{dH_i}{dt} &= \gamma\,I_i - \omega\,H_i, \qquad t\in(0,T]\\
\frac{dR_i}{dt} &= (1-f(S_i,V_i))\,\omega\,H_i - \mu_R\,R_i,\\
\frac{dD_i}{dt} &= f(S_i,V_i)\,\omega\,H_i,\\
\frac{dV_i}{dt} &= -\left(\sum_{k=1}^{K}\left(\sum_{j=1}^{M} c(t)\,\beta_{ij}^k I_j\right)\right)\frac{\sigma V_i}{N_i} + \rho_i\,\frac{S_i}{S_i+R_i} - \mu_V\,V_i,\\
S_i(0) &= S_{i_0}, \quad E_i^k(0) = E_{i_0}^k, \quad I_i(0) = I_{i_0}, \quad H_i(0) = H_{i_0},\\
& \qquad R_i(0) = R_{i_0}, \quad D_i(0) = D_{i_0}, \quad V_i(0) = V_{i_0}
\end{aligned}
\tag{8}
$$

$\forall\, i = 1,\dots,N_a.$

3. Results

We report numerical results obtained in different scenarios for both the global and regional Italian levels. Our aim is to capture how COVID-19 developed in the different contexts of exposition among the different age groups and to assess the validity of the proposed novel compartmental model. For each period selected, accurate research was carried out to set the scenario parameters, taking into account the containment measures in force and their variations in the respective time-frame.

In particular, in Section 3.1, we present the results set at the Italian national level from September 2020 to July 2021, in Section 3.2, we analyze the same period in Lombardy and Lazio, while in Section 3.3, we report the results for the entire Country up to December 2021, in order to evaluate the impact of the Green Pass measure.

3.1. September 2020–July 2021: Italy

At the beginning of the period of interest, very few NPI restrictions were in force, and, in particular, schools were open. With the increase in infections, regional restrictions were introduced starting from November, with the classification in three colors according to the risk: yellow, orange, and red.

For the first calibration, we set $\theta = 1$ and $\mu_R = 0$, so we consider that once a positive diagnosis is received, vaccines are totally ineffective in reducing deaths, and that recovered individuals become immune. Note that if we consider $\theta = 1$, the function $f(S, V; \tau)$ defined in (2) is equal to the *Infectious Fatality Rate*.

As we can see in Figure 9, the amount of Deceased individuals matches with actual monitoring, showing the reasonable behavior of the curve of positive individuals. Indeed, it is possible to see that the $I + H$ curve follows the trend of the positives given by DPC. The gap between the two curves is due to monitoring uncertainty: the SEIHRDV model does not distinguish detected from undetected individuals.

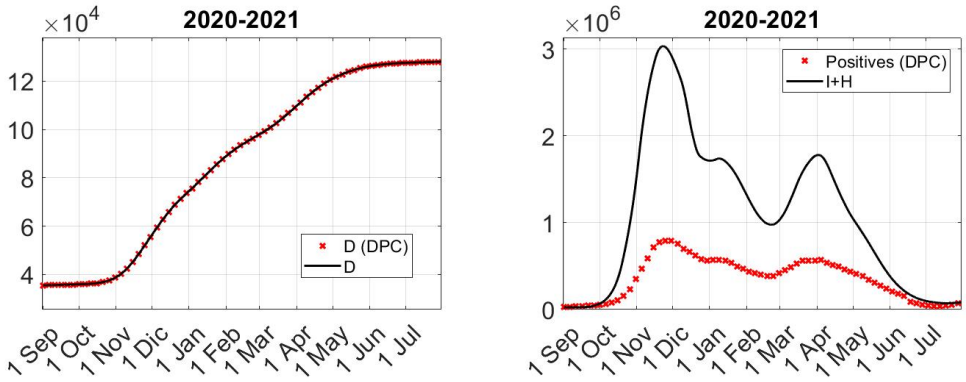


Figure 9. Calibration results in Italy: the calibration on reported deceased (**left**); the sum of Infectious and Healing individuals estimated by the model compared with reported positives (**right**).

In Figure 10, we compare Deceased individuals divided by age groups, since we are able to reconstruct the IFR for each age class. The calibration procedure prioritizes aligning the predicted deaths with the highest numbers, which occur primarily among elderly age groups. This focus is crucial for accurately calibrating the model and predicting disease spread. In fact, the stratification of deaths in our model closely matches the available data, particularly for the elderly, who account for the majority of fatalities. Mismatches are observed in the younger age groups, but these groups are less numerous and have a smaller weight in the calibration process. In Figure 11, the curves of positives individuals (i.e., Infectious and Healing individuals) estimated by the SEIHRDV multi-age and multi-context model follow the trend of the data. As in Figure 9, the gap between the curves and the data is motivated by the limitations in monitoring. In particular, in the 70+ age group, we observed that the estimated curve and the data are similar; this is probably due to the fact that older individuals are more often symptomatic than other age groups, and thus they are more easily detected.

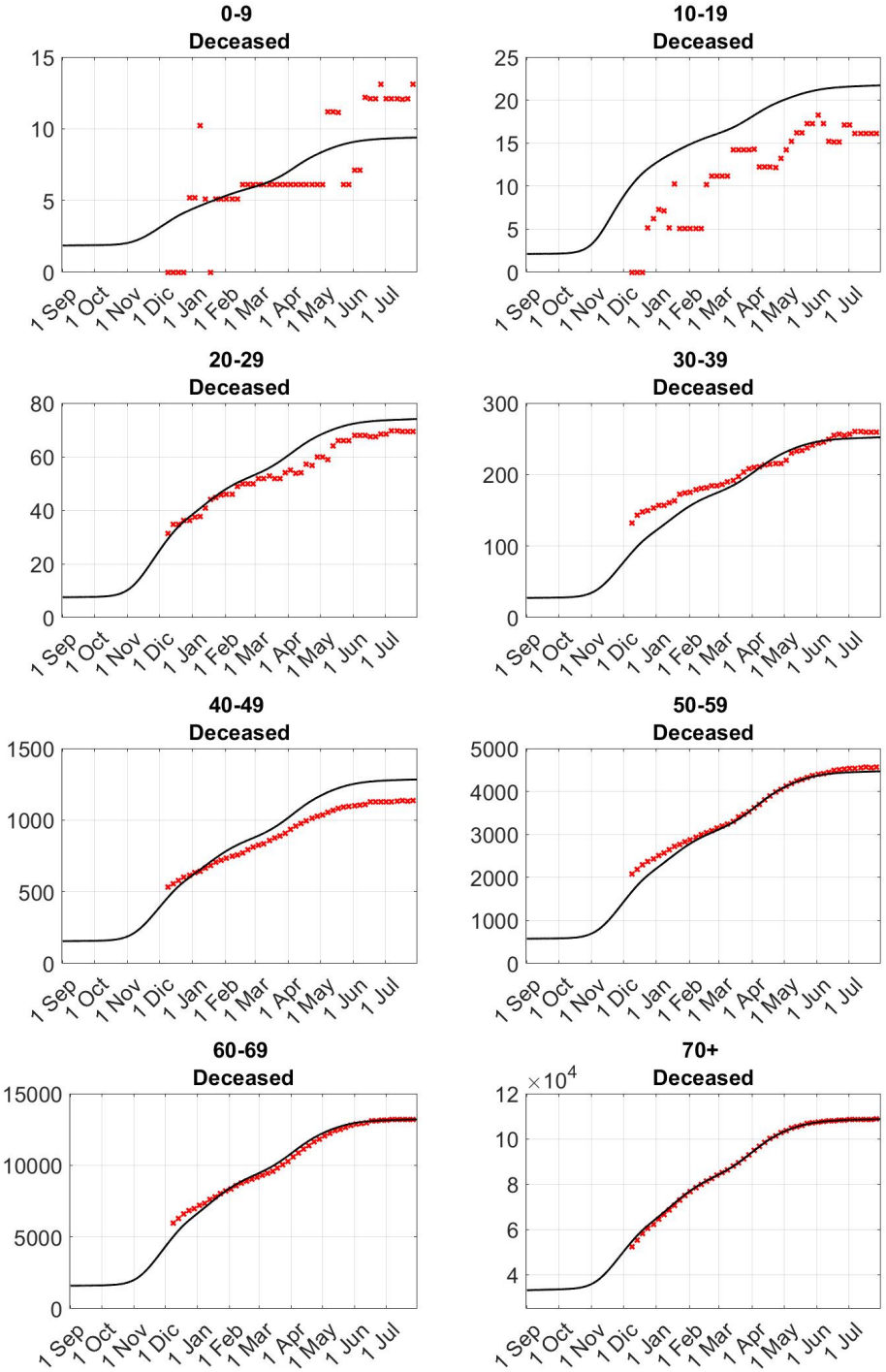


Figure 10. Deceased individuals in Italy from September 2020 to July 2021, estimated by the SEIHRDV multi-age and multi-context model divided by age group, compared with data (in red).

The peculiarity of the SEIHRDV multi-age and multi-context is that we can observe how Exposed individuals are distributed in each age group and the context of exposition. In Figure 12, we show the age classes (top left) and contexts of exposition (top right) of exposed individuals, while at the bottom, we have the distribution of age groups (bottom left) and context of exposition (bottom right) in the exposed compartment. In this way, we can interpret the numerical results in light of the specific NPIs placed in action and evaluate the impact of specific interventions. For instance, in the middle of September 2020, schools were totally open. This led to an increase of cases in the younger age groups until the beginning of November, when some restrictions where applied with the introduction of

colored zones. Since then, the most exposed age groups were 40–49 and 50–59. For what concerns the contexts of exposition, we can see that in the first part of the growth of the curve, "leisure" was the context with the greatest exposures. Then, with the introduction of the containment measures in November, the context in which most infections occur was the "work" sector. In the same way, the infections in the "school" context, which were growing, began to decline and then remained more or less constant (with an exception for the Christmas holidays). School-related restrictions particularly affected a part of middle and high school students.

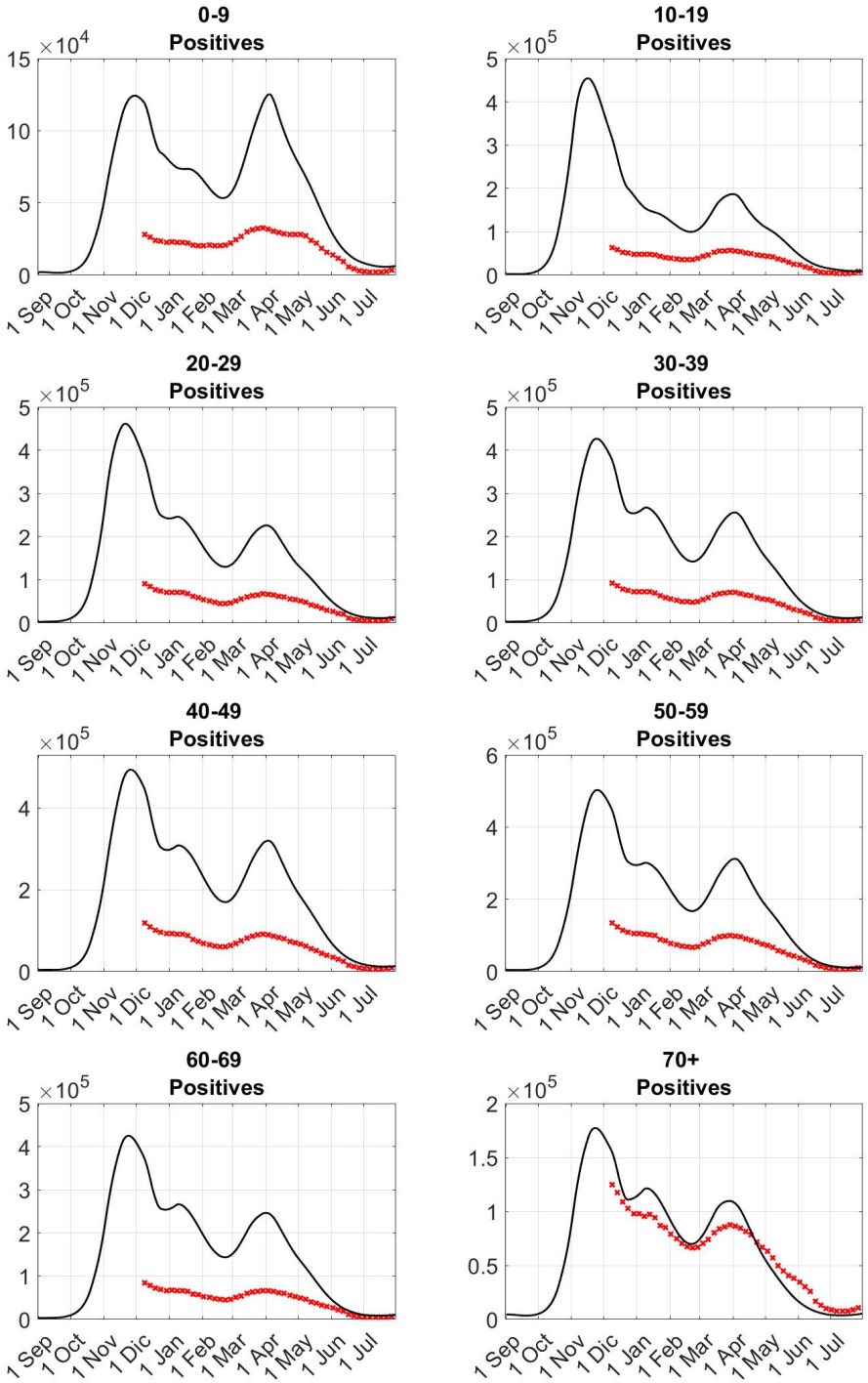


Figure 11. Positives ($I + H$) in Italy from September 2020 to July 2021, estimated by the SEIHRDV multi-age and multi-context model divided by age group, compared with data (in red).

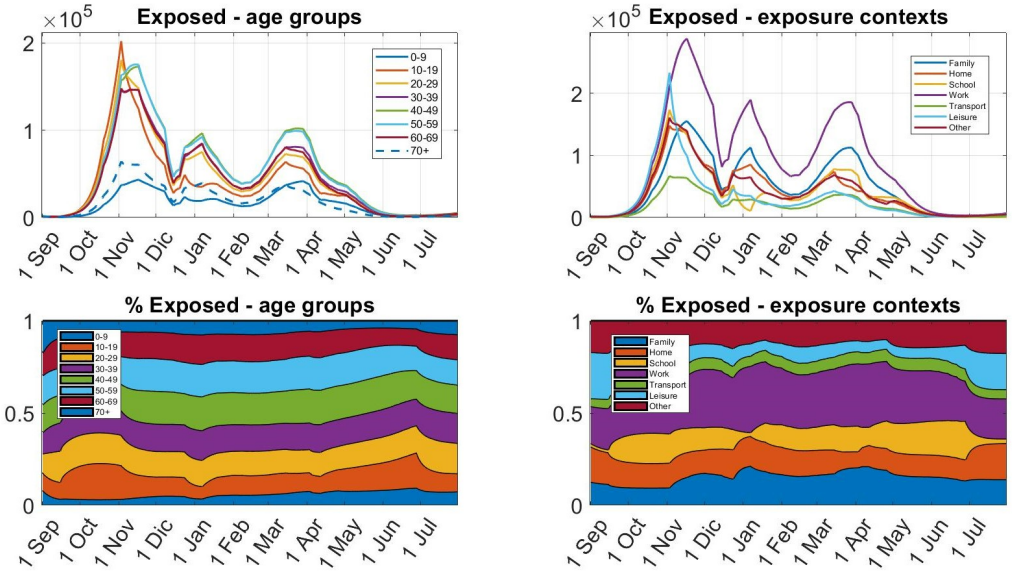


Figure 12. Exposed in Italy from September 2020 to July 2021: at the top, evolution of the exposed individuals divided by age group (top left) and context of exposition (top right); at the bottom, distribution of age groups (bottom left) and contexts of exposition (bottom right) in the exposed compartment.

For the sake of completeness, we repeated the numerical tests by imposing $\theta = 0.8$. We estimated this value of θ, that is, the rate of inefficacy of vaccination in the reduction of death, from ISS data reported in [43]. We obtained similar results. In particular, we can see a difference in the Recovered compartment: if fewer individuals die, more individuals will have recovered (Figure 13).

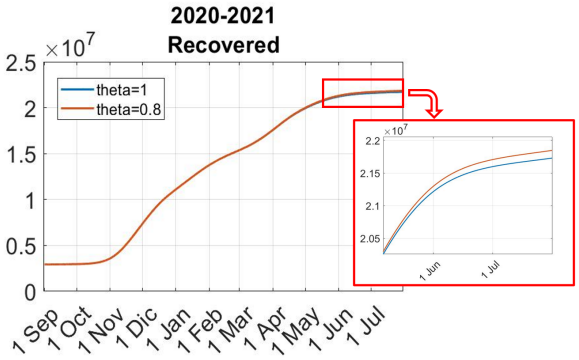


Figure 13. Curves of Recovered with $\theta = 1$ and $\theta = 0.8$, compared over the whole time period.

3.2. September 2020–July 2021: Regions Lombardy and Lazio

The trend in the national epidemic curve is influenced by the trends in the individual regions. In fact, the situation may be different in each region, depending on the average age of individuals, daily habits, hospital situation, and climatic situation. For this reason, the NPIs in the chosen time period were adopted on a regional scale. Hence, we analyzed what happened in two of the most populous Italian regions: Lombardy and Lazio. As we did in Section 3.1, we set up the scenario and the initial conditions by imposing $\theta = 1$ and $\mu_R = 0$.

3.2.1. Lombardy

As we can see in Figure 14, the amount of Deceased individuals matches with the actual data, also showing a reasonable behavior of positive individuals in Lombardy.

The $I + H$ curve follows the trend in the positives given by DPC. Even in this case, the gap between the two curves is due to the accuracy of the detection. In Figures 15 and 16, we report Deceased individuals and positive individuals divided by age groups.

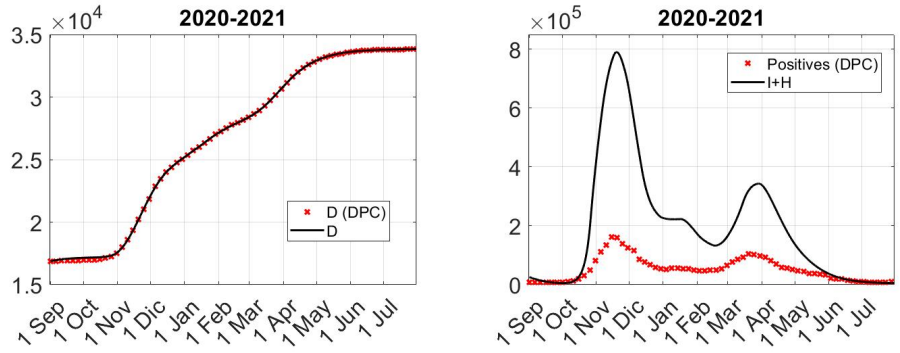


Figure 14. Calibration results in Lombardy: the calibration on reported Deceased on the **left**; the sum of Infectious and Healing estimated by the model compared with reported positives on the **right**.

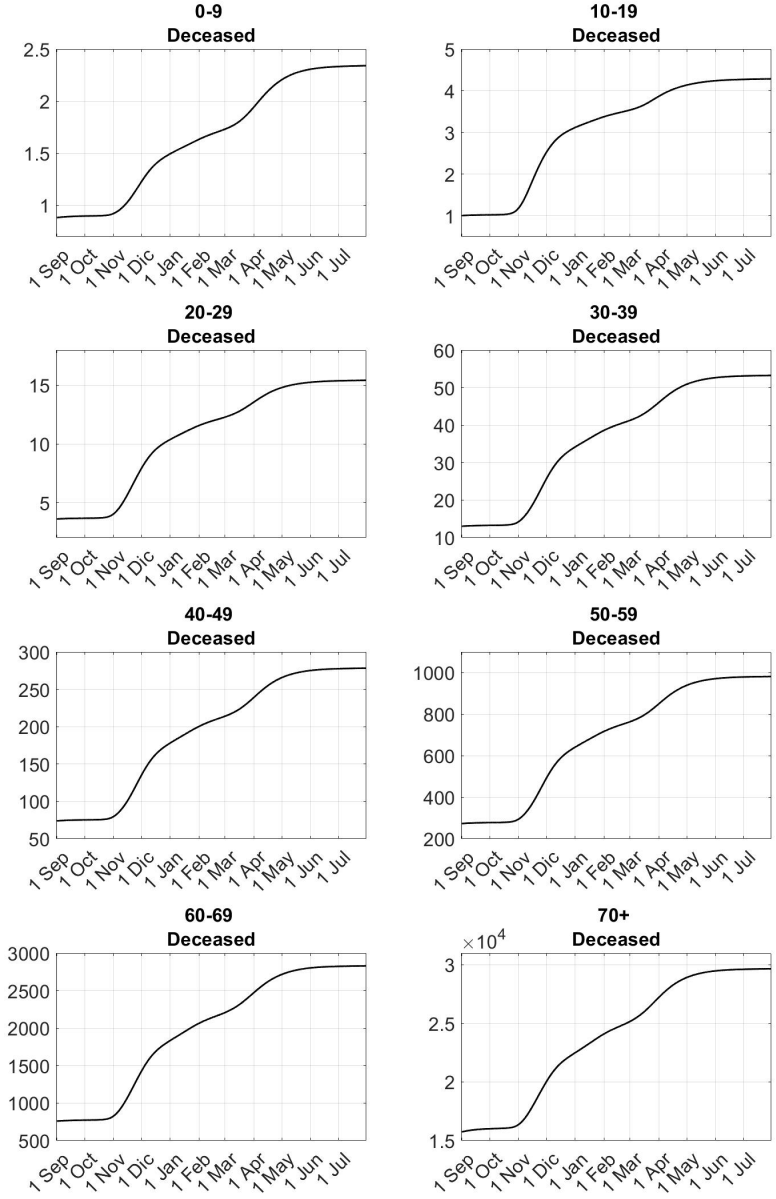


Figure 15. Deceased in Lombardy estimated by SEIHRDV multi-age/multi-context model divided by age group.

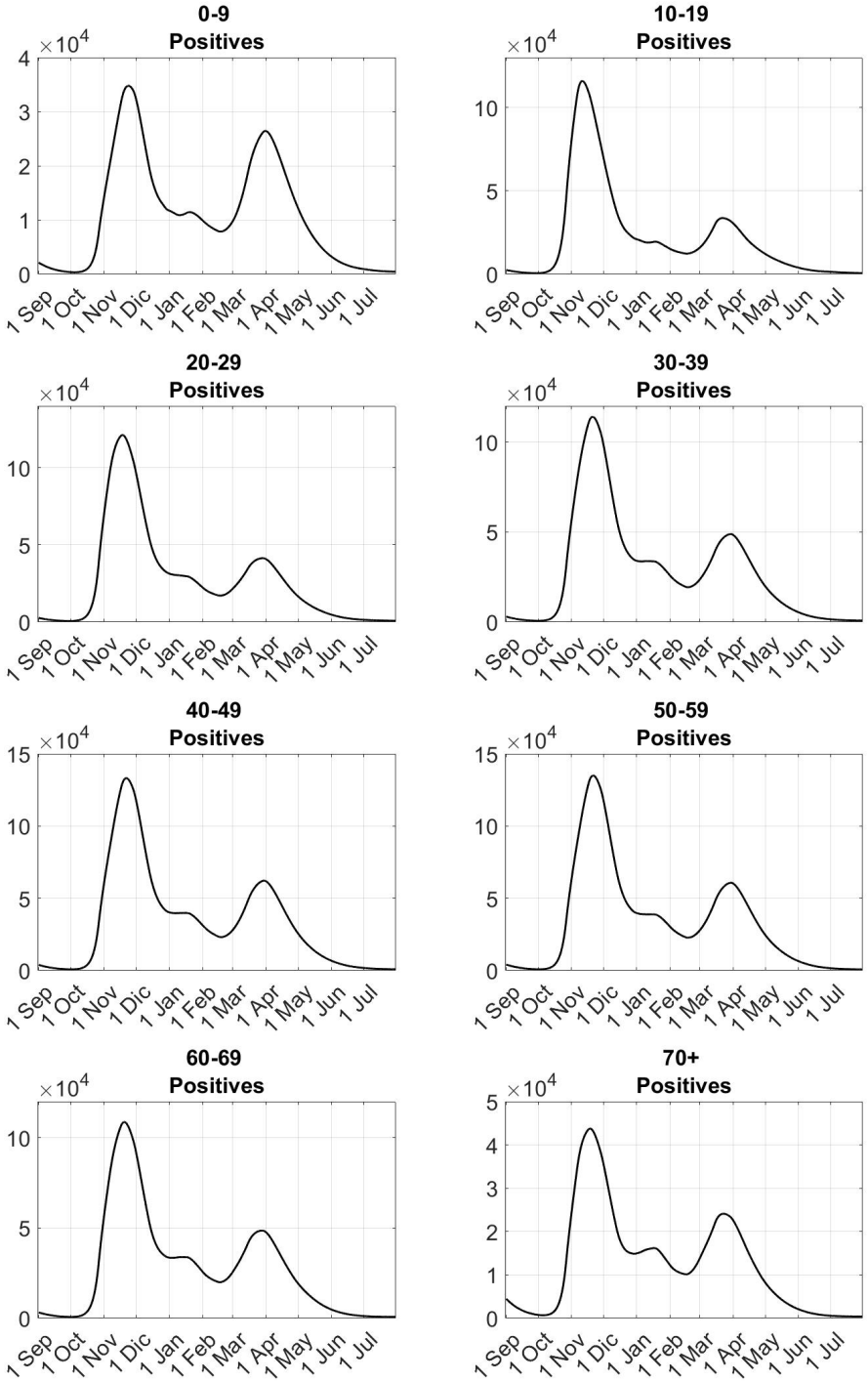


Figure 16. Positives ($I + H$) in Lombardy, estimated by the SEIHRDV multi-age/multi-context model divided by age group.

By using the SEIHRDV multi-age and multi-context model, we were able to track the evolution of infections in each age group and each context of exposition. In Figure 17, we report the amount of Exposed divided by age groups and context of exposition, while at the bottom, we can see how the Exposed (and therefore the infections) are divided into age groups and contexts of exposition. As we expected, the curves in Figure 17 follow different trends compared to the national curve of the Exposed individuals (Figure 12).

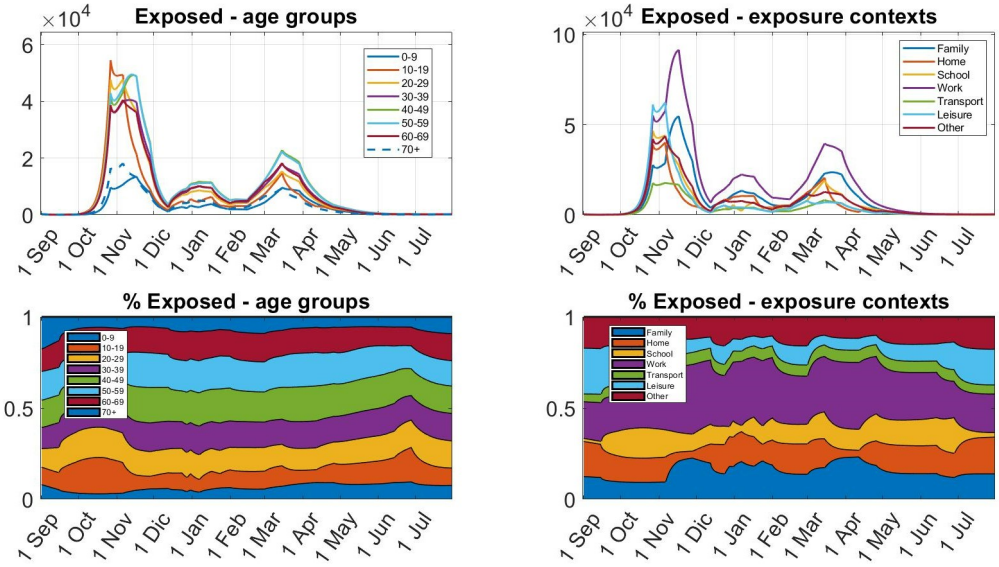


Figure 17. Exposed in Lombardy: at the top, evolution of the exposed individuals divided by age group (top left) and context of exposition (top right); at the bottom, distribution of age groups (bottom left) and contexts of exposition (bottom right) in the exposed compartment.

3.2.2. Lazio

In Figure 18, we observe that even in this case, deceased individuals match the actual data. The curve of positives in the same figure follows the trend of the positives given by DPC, with the usual gap ascribed to monitoring uncertainty. In Figures 19 and 20, we report deceased individuals and positive individuals divided by age groups.

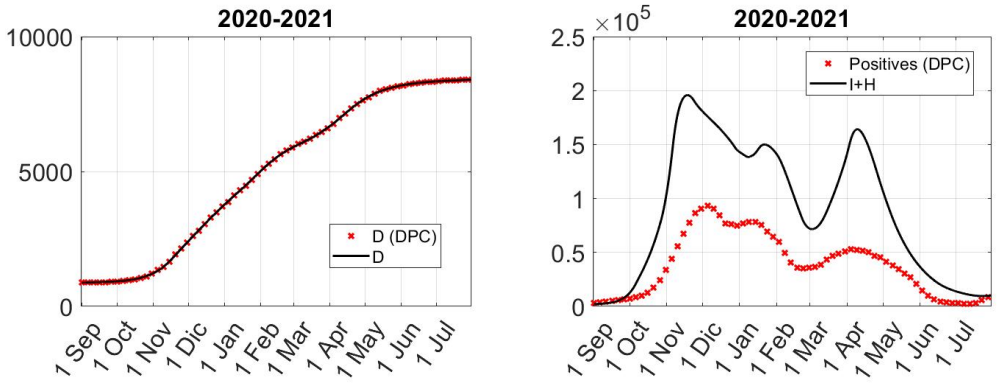


Figure 18. Calibration results in Lazio: the calibration on reported deceased at the **left**; the sum of Infectious and Healing estimated by the model compared with reported positives at the **right**.

In Figure 21 the amount of exposed is represented divided by age groups and context of exposition, together with how age groups and contexts of exposition are distributed in the exposed compartment. The curves in Figure 21 are different from both the national curves of exposed (Figure 12) and the Lombardy curves (Figure 17).

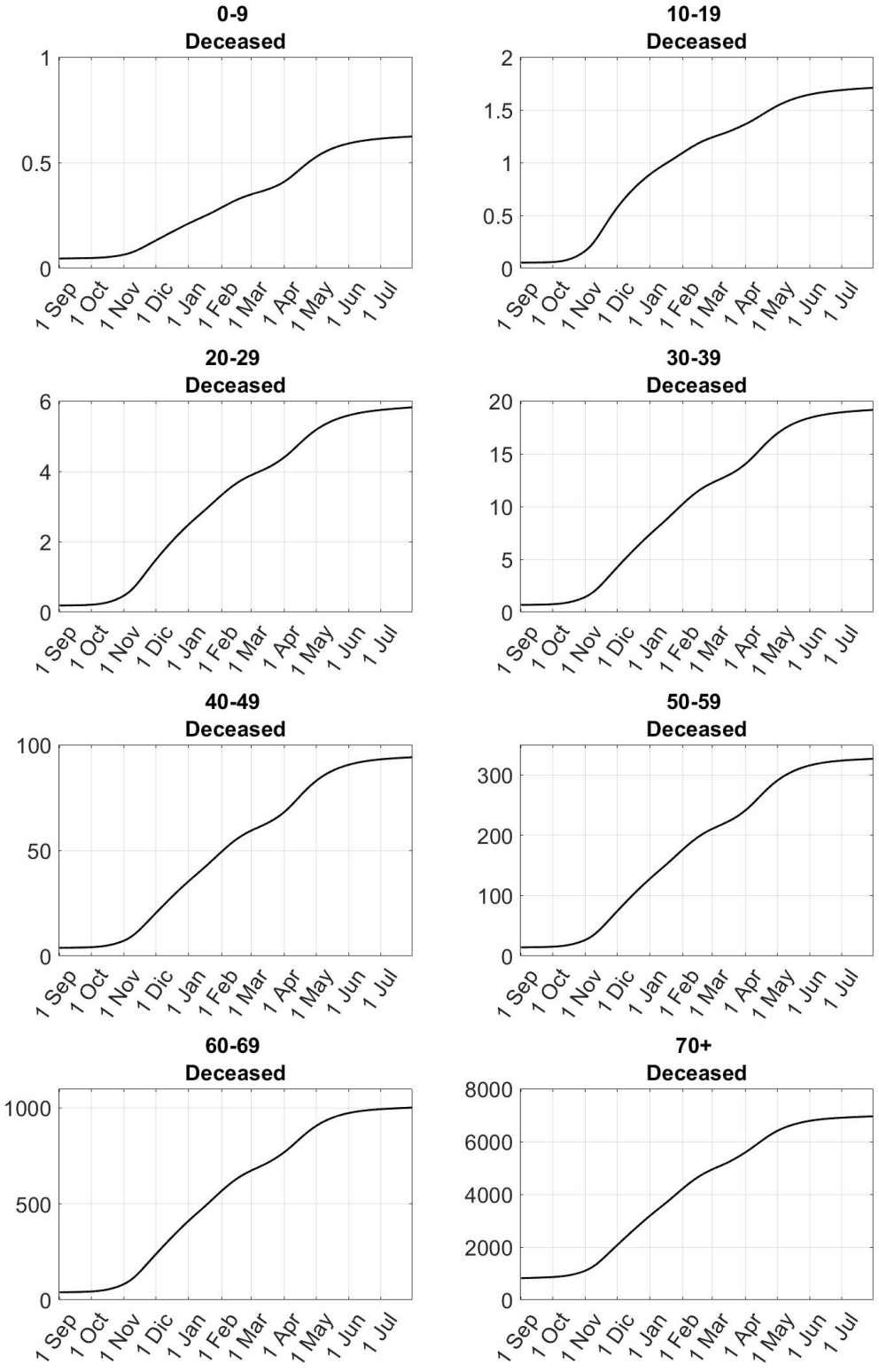


Figure 19. Deceased in Lazio, estimated by the SEIHRDV multi-age/multi-context model divided by age group.

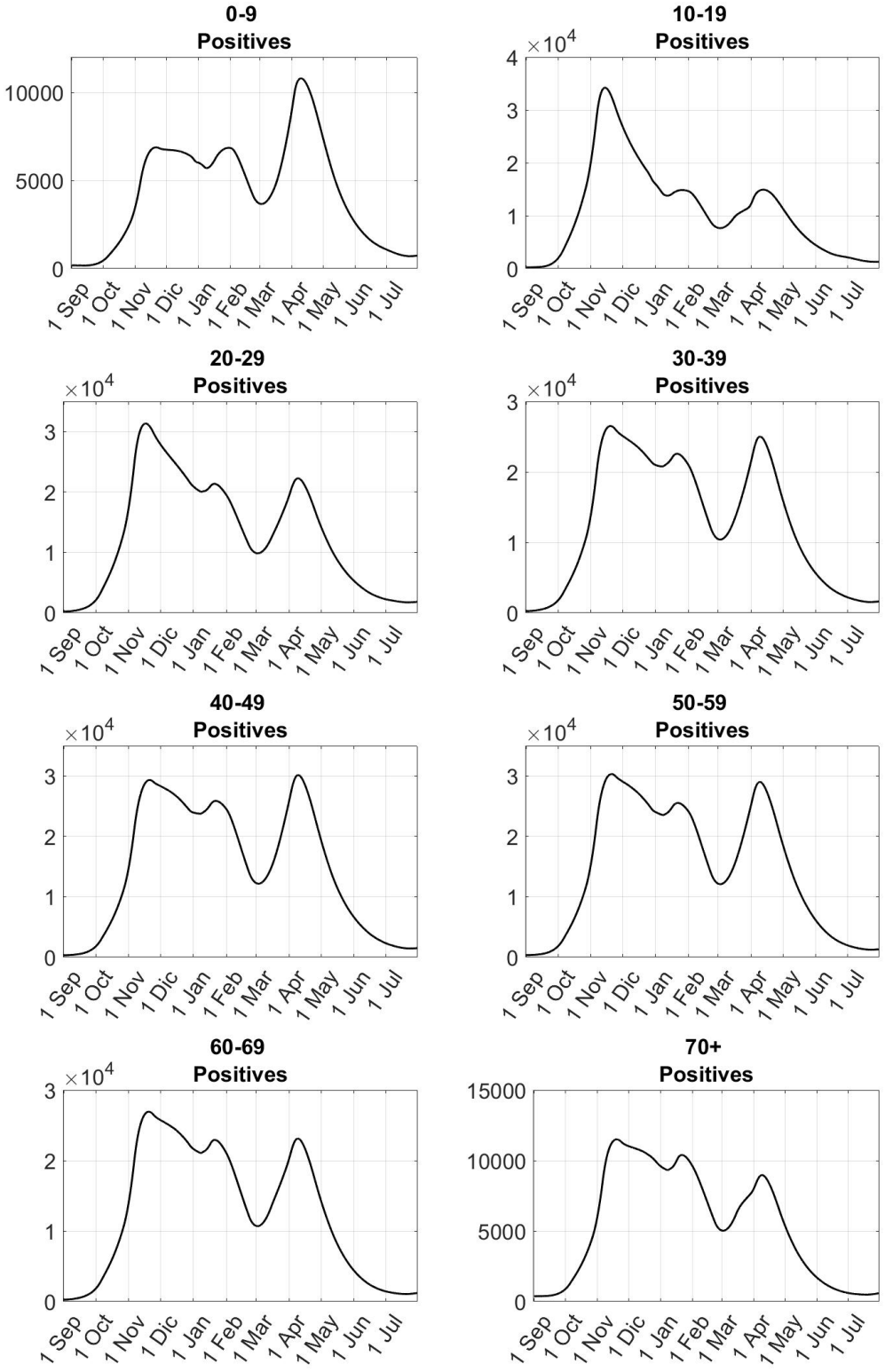


Figure 20. Positives ($I + H$) in Lazio, estimated by the SEIHRDV multi-age/multi-context model divided by age group.

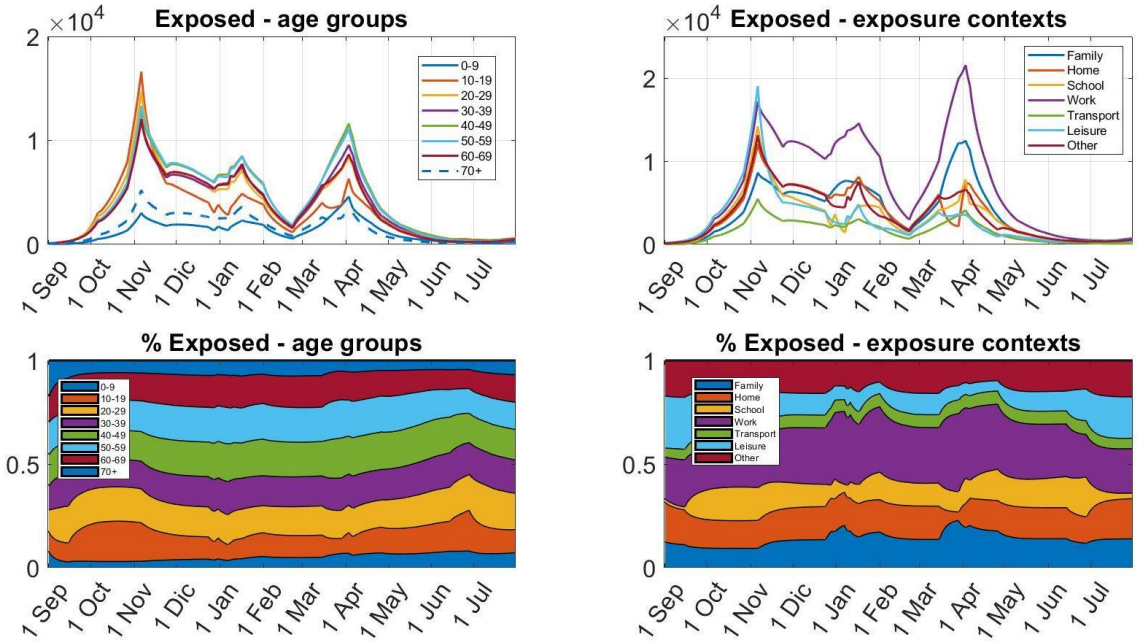


Figure 21. Exposed in Lazio: at the top, evolution of the exposed individuals divided by age group (top left) and context of exposition (top right); at the bottom, distribution of age groups (bottom left) and contexts of exposition (bottom right) in the exposed compartment.

3.3. September 2020–December 2021: Italy

In this section, we take into account the Green Pass restrictions as introduced in Section 2.4.3. To set the scenarios, until the end of July, we used the same setting imposed in Section 3.1, while from August onward, we took into account the new rules related to the Green Pass described below:

- From August 6 to September 12: Green Pass requirement for indoor restaurants, indoor pubs, discos, indoor sports and various events (concerts, museums, cinemas, stadium, shows, theaters);
- From September 13 to October 14: Green Pass requirement also extended to school staff and university students;
- From October 15 onward: Green Pass requirement also extended to workers.

For the sake of simplicity, we considered only vaccinated individuals as Green Pass holders, since our model does not explicitly monitor swabs. We considered the same initial condition of the first calibration seen in Section 3.1, using a non-zero rate of end of immunity for recovered individuals since we considered a time period longer than a year.

In Figure 22, we show the trend of positive individuals in the Green Pass case, and observe that it matches the available data. Since the gap between the curve and the data is smaller from July, we can deduce that a better monitoring policy was induced by the introduction of the Green Pass obligation (notice that the Green Pass could also be granted if swabs are negative). The curve also catches the rise in cases that began in mid-October. Figure 23 shows the distribution of reported and predicted Deceased individuals across age groups. As highlighted in Figure 10, the model's calibration procedure results in a much better match for the elderly age groups, as it prioritizes deaths in those groups with the highest numbers, compared to the younger age groups.

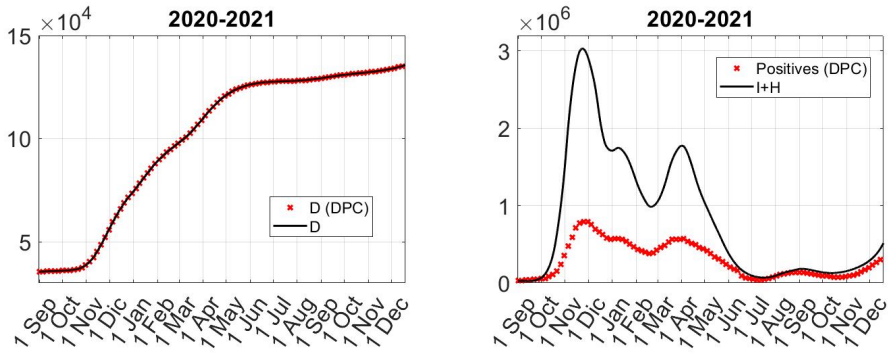


Figure 22. Calibration results in Italy: the calibration on reported deceased at the **left**; the sum of Infectious and Healing estimated by the model compared with reported positives at the **right**, introducing Green Pass containment measures.

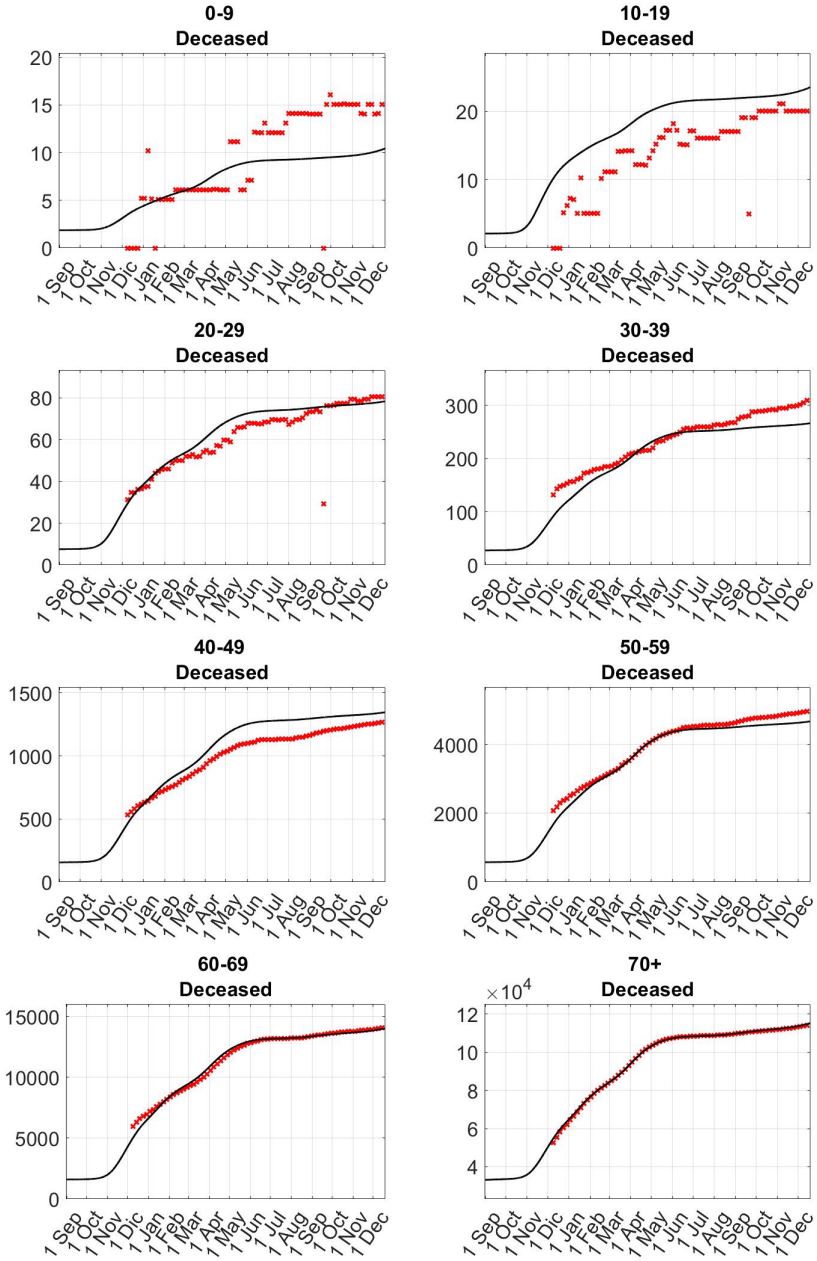


Figure 23. Deceased in Italy, estimated by the SEIHRDV multi-age/multi-context model divided by age group, introducing Green Pass containment measures.

In Figure 24, it is possible to observe differences between the age groups in this last time period. In particular, from the SEIHRDV multi-age/multi-context model, it is possible to see a significant growth in the age groups 0–9 and 10–19, possibly due to the school reopening. In fact, in July and August, schools closed, as shown in the distribution of Exposed in the different contexts of exposure (Figure 25): starting in September, the Exposed in the context "school" started to grow again. In particular, the age groups most affected by school reopening were indeed those aging 0–9 and 10–19 (as can be seen in Figure 25), which are also those less vaccinated (the vaccination campaign concerned those over 12 years old).

Finally, we conclude that Green Pass NPIs had a greater impact in the context of exposition of *work*, and in a lighter way in *leisure*, as we can see in Figure 25. On the other hand, an increase in the rate of exposure to the virus was observed in contexts such as *school* and *home*.

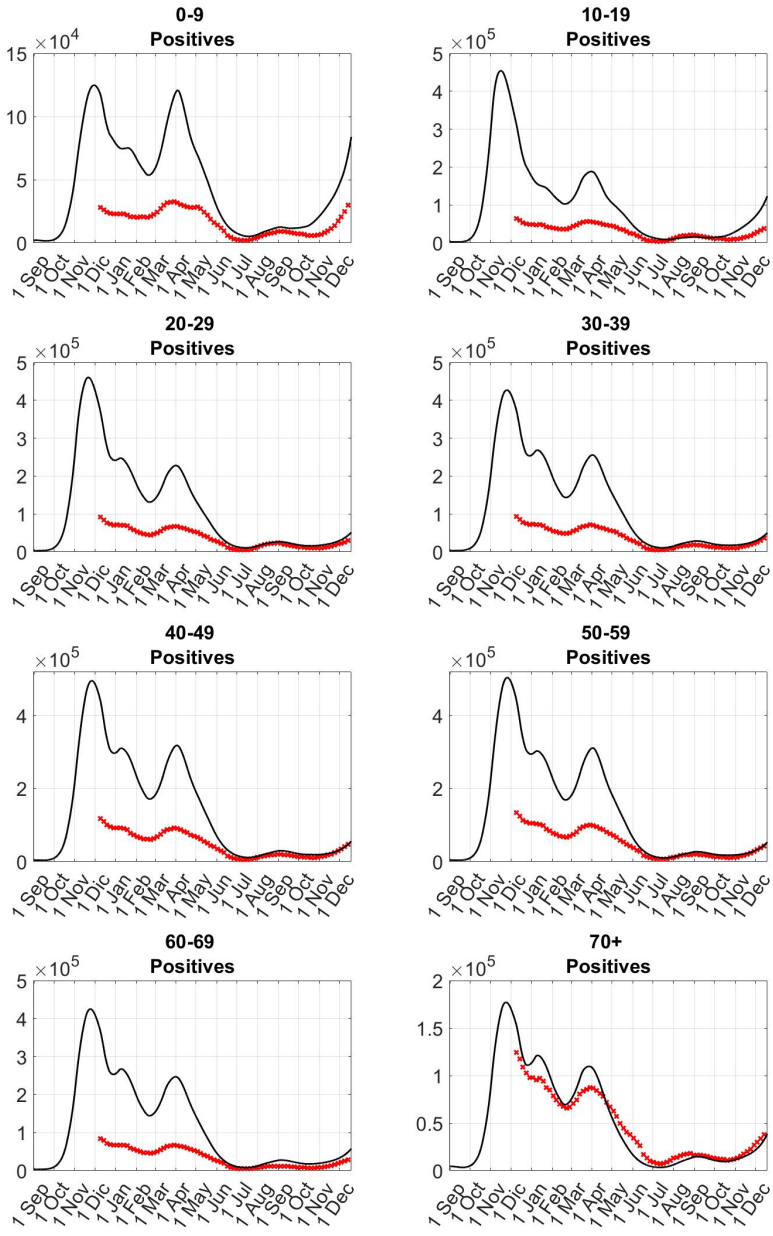


Figure 24. Positives ($I + H$) in Italy, estimated by the SEIHRDV multi-age/multi-context model divided by age group, introducing Green Pass containment measures.

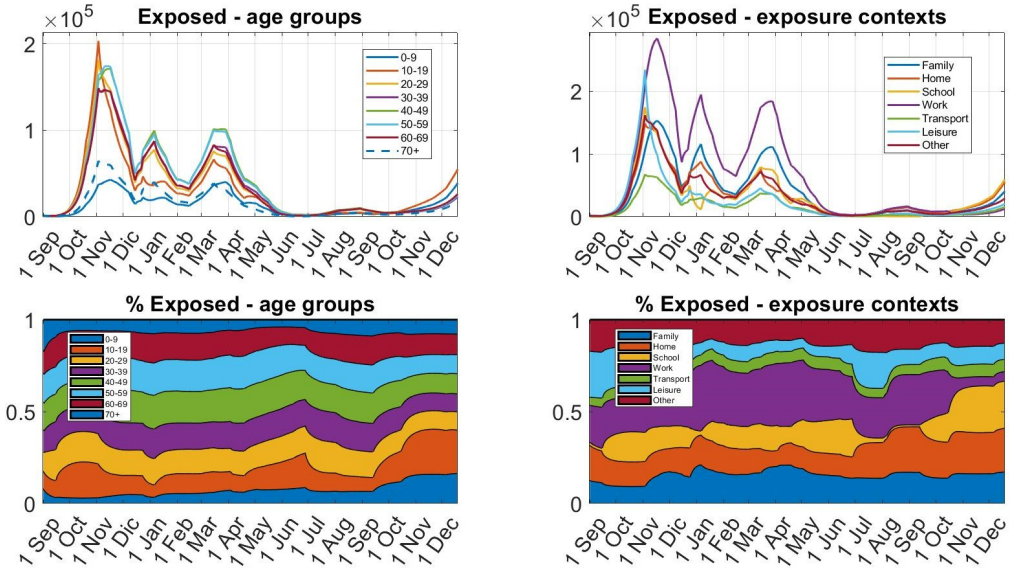


Figure 25. Exposed in Italy with Green Pass containment measures: evolution of the exposed individuals divided by age group (top left) and context of exposition (top right), distribution of age groups (bottom left) and contexts of exposition (bottom right) in the exposed compartment.

4. Conclusions and Perspectives

We introduced a new mathematical model to describe the COVID-19 epidemic in Italy during the years 2020 and 2021. This is a multi-age and multi-context SEIHRDV model, constituted by seven compartments: Susceptible individuals S, Exposed individuals E, Infectious individuals I, Healing individuals H, Recovered individuals R, Dead individuals D, and Vaccinated individuals V. This model was specifically designed to analyze the spread of COVID-19 in Italy between September 2020 and July 2021, with a focus on predicting epidemic dynamics rather than individual health outcomes. Its primary goal was to support authorities in decision making, particularly in NPIs targeting different exposure contexts and age groups.

By tracking infection patterns across age groups and exposure settings, we used SEIHRDV to reconstruct the spread of COVID-19 in Lombardy and Lazio while accounting for key factors such as the vaccination campaign and Green Pass interventions. The model enables the assessment of NPIs' impact across different contexts in a heterogeneous manner. Importantly, our numerical results, differentiated by age and exposure contexts, provide valuable insights into which age groups and contexts posed the highest epidemiological risks. This detailed analysis was instrumental in understanding transmission dynamics and informing targeted intervention strategies.

The model was validated using data from the Dipartimento di Protezione Civile, Italy, which were also used to calibrate the model parameters through a standard least squares optimization scheme. Given the uncertainty and under-reporting of real positive cases, we focused on data regarding deceased individuals—widely regarded as the most reliable and least affected by monitoring uncertainties. This approach aimed to reduce bias and ensure more accurate calibration of the model.

The SEIHRDV multi-age and multi-context model provided a valuable framework for analyzing differences in behavior across age groups and understanding how infections spread within various exposure settings. For example, the model revealed that exposures and infections among younger age groups largely went undetected and were likely transmitted—plausibly through family contacts—to older age groups. In these elderly populations, infections became more noticeable due to their severe impact, such

as hospitalizations and other complications. We believe the model also revealed that a significant number of exposures likely occurred in settings primarily attended by younger populations—such as schools, social gathering places, and workplaces—but largely went undetected until the virus reached elderly age groups, likely through family contacts.

The model, originally designed to study COVID-19 spread in Italy from 2020 to fall 2021, can be adapted for future outbreaks. Potential enhancements include adding compartments to account for fully vaccinated individuals or tracking undetected cases, as achieved in other studies. Despite its current limitations, we are confident that this model serves as a fundamental tool for policymakers, providing reliable scenario analyses for future epidemic responses.

Author Contributions: Conceptualization, L.D.; methodology, L.D., N.P., A.Q. and G.V.; software, L.D. and G.V.; validation, L.D., N.P., A.Q. and G.V.; formal analysis, L.D., N.P., A.Q., G.V. and G.Z.; writing—original draft preparation, L.D., N.P. and G.V.; writing—review and editing, L.D., N.P., A.Q., G.V. and G.Z.; visualization, L.D., G.V. and G.Z.; supervision, A.Q. All authors have read and agreed to the published version of the manuscript.

Funding: This research received no external funding.

Data Availability Statement: The results in this study were obtained by applying the proposed models to data from the following available sources: Dipartimento di Protezione Civile Italiana https://github.com/italia/covid19-opendata-vaccini; Dipartimento di Protezione Civile Italiana https://github.com/pcm-dpc/COVID-19; Presidenza del Consiglio dei Ministri, Comitato Tecnico Scientifico https://emergenze.protezionecivile.gov.it/it/sanitarie/coronavirus/verbali-comitato-tecnico-scientifico/ (all accessed on 1 March 2021).

Acknowledgments: L.D., N.P. and G.Z. acknowledge their membership to INdAM group GNCS—Gruppo Nazionale per il Calcolo Scientifico (National Group for Scientific Computing, Italy). The present research is part of the activities of "Dipartimento di Eccellenza 2023–2027", MUR, Italy, Department of Mathematics, Politecnico di Milano.

Conflicts of Interest: The authors declare no conflicts of interest.

References

1. Parolini, N.; Ardenghi, G.; Dede', L.; Quarteroni, A. A mathematical dashboard for the analysis of Italian COVID-19 epidemic data. *Int. J. Numer. Methods Biomed. Eng.* **2021**, *37*, e3513. [CrossRef] [PubMed]
2. Kermack, W.; McKendrick, A.G. A contribution to the mathematical theory of epidemics. *Proc. R. Soc. Lond. Ser. Contain. Pap. Math. Phys. Character* **1927**, *115*, 700–721.
3. Wangersky, P.J. Lotka-Volterra population models. *Annu. Rev. Ecol. Syst.* **1978**, *9*, 189–218. [CrossRef]
4. Bertuzzo, E.; Mari, L.; Pasetto, D.; Miccoli, S.; Casagrandi, R.; Gatto, M.; Rinaldo, A. The geography of COVID-19 spread in Italy and implications for the relaxation of confinement measures. *Nat. Commun.* **2020**, *11*, 4264. [CrossRef] [PubMed]
5. Della Rossa, F.; Salzano, D.; Di Meglio, A.; De Lellis, F.; Coraggio, M.; Calabrese, C.; Guarino, A.; Cardona-Rivera, R.; De Lellis, P.; Liuzza, D.; et al. A network model of Italy shows that intermittent regional strategies can alleviate the COVID-19 epidemic. *Nat. Commun.* **2020**, *11*, 5106. [CrossRef]
6. Bertaglia, G.; Pareschi, L. Hyperbolic models for the spread of epidemics on networks: Kinetic description and numerical methods. *ESAIM Math. Model. Numer. Anal.* **2021**, *55*, 381–407. [CrossRef]
7. Dimarco, G.; Perthame, B.; Toscani, G.; Zanella, M. Kinetic models for epidemic dynamics with social heterogeneity. *J. Math. Biol.* **2021**, *83*, 4. [CrossRef] [PubMed]
8. Ram, V.; Schaposnik, L.P. A modified age-structured SIR model for COVID-19 type viruses. *Sci. Rep.* **2021**, *11*, 15194. [CrossRef]
9. Parolini, N.; Dede', L.; Antonietti, P.; Ardenghi, G.; Manzoni, A.; Miglio, E.; Pugliese, A.; Verani, M.; Quarteroni, A. SUIHTER: A new mathematical model for COVID-19. Application to the analysis of the second epidemic outbreak in Italy. *Proc. R. Soc. A* **2021**, *477*, 20210027. [CrossRef] [PubMed]
10. Parolini, N.; Dede', L.; Ardenghi, G.; Quarteroni, A. Modelling the COVID-19 epidemic and the vaccination campaign in Italy by the SUIHTER model. *Infect. Dis. Model.* **2022**, *7*, 45–63. [CrossRef]

11. Gatto, M.; Bertuzzo, E.; Mari, L.; Miccoli, S.; Carraro, L.; Casagrandi, R.; Rinaldo, A. Spread and dynamics of the COVID-19 epidemic in Italy: Effects of emergency containment measures. *Proc. Natl. Acad. Sci. USA* **2020**, *117*, 10484–10491. [CrossRef] [PubMed]
12. Ivorra, B.; Ferrández, M.R.; Vela-Pérez, M.; Ramos, A.M. Mathematical modeling of the spread of the coronavirus disease 2019 (COVID-19) taking into account the undetected infections. The case of China. *Commun. Nonlinear Sci. Numer. Simul.* **2020**, *88*, 105303. [CrossRef] [PubMed]
13. Bertaglia, G.; Pareschi, L. Hyperbolic compartmental models for epidemic spread on networks with uncertain data: Application to the emergence of COVID-19 in Italy. *Math. Model. Methods Appl. Sci.* **2021**, *31*, 2495–2531. [CrossRef]
14. Lekone, P.; Finkenstädt, B. Statistical inference in a stochastic epidemic SEIR model with control intervention: Ebola as a case study. *Biometrics* **2006**, *62*, 1170–1177. [CrossRef]
15. Zimmer, C.; Yaesoubi, R.; Cohen, T. A likelihood approach for real-time calibration of stochastic compartmental epidemic models. *PLoS Comput. Biol.* **2017**, *13*, e1005257. [CrossRef] [PubMed]
16. Kerr, C.; Stuart, R.; Mistry, D.; Abeysuriya, R.; Rosenfeld, K.; Hart, G.; Núñez, R.; Cohen, J.; Selvaraj, P.; Hagedorn, B.; et al. Covasim: An agent-based model of COVID-19 dynamics and interventions. *PLoS Comput. Biol.* **2021**, *17*, e1009149. [CrossRef]
17. Lasser, J.; Sorger, J.; Richter, L.; Thurner, S.; Schmid, D.; Klimek, P. Assessing the impact of SARS-CoV-2 prevention measures in Austrian schools using agent-based simulations and cluster tracing data. *Nat. Commun.* **2022**, *13*, 554. [CrossRef]
18. Hoertel, N.; Blachier, M.; Blanco, C.; Olfson, M.; Massetti, M.; Rico, M.; Limosin, F.; Leleu, H. A stochastic agent-based model of the SARS-CoV-2 epidemic in France. *Nat. Med.* **2020**, *26*, 1417–1421. [CrossRef] [PubMed]
19. Millevoi, C.; Pasetto, D.; Ferronato, M. A Physics-Informed Neural Network approach for compartmental epidemiological models. *PLoS Comput. Biol.* **2024**, *20*, e1012387. [CrossRef]
20. Shaier, S.; Raissi, M.; Seshaiyer, P. Data-Driven Approaches for Predicting Spread of Infectious Diseases Through DINNs: Disease Informed Neural Networks. *Lett. Biomath.* **2022**, *9*, 71–105.
21. Bertaglia, G.; Lu, C.; Pareschi, L.; Zhu, X. Asymptotic-Preserving Neural Networks for multiscale hyperbolic models of epidemic spread. *Math. Model. Methods Appl. Sci.* **2022**, *32*, 1949–1985. [CrossRef]
22. Olumoyin, K.; Khaliq, A.; Furati, K. Data-driven deep-learning algorithm for asymptomatic COVID-19 model with varying mitigation measures and transmission rate. *Epidemiologia* **2021**, *2*, 471–489. [CrossRef]
23. Ziarelli, G.; Parolini, N.; Verani, M. Learning epidemic trajectories through Kernel Operator Learning: From modelling to optimal control. *arXiv* **2024**, arXiv:2404.11130.
24. Ziarelli, G.; Pagani, S.; Parolini, N.; Regazzoni, F.; Verani, M. A model learning framework for inferring the dynamics of transmission rate depending on exogenous variables for epidemic forecasts. *arXiv* **2024**, arXiv:2410.11545. [CrossRef]
25. Mari, L.; Casagrandi, R.; Bertuzzo, E.; Pasetto, D.; Miccoli, S.; Rinaldo, A.; Gatto, M. The epidemicity index of recurrent SARS-CoV-2 infections. *Nat. Commun.* **2021**, *12*, 2752. [CrossRef] [PubMed]
26. Marziano, V.; Guzzetta, G.; Mammone, A.; Riccardo, F.; Poletti, P.; Trentini, F.; Manica, M.; Siddu, A.; Bella, A.; Stefanelli, P.; et al. The effect of COVID-19 vaccination in Italy and perspectives for living with the virus. *Nat. Commun.* **2021**, *12*, 7272. [CrossRef]
27. Marziano, V.; Guzzetta, G.; Rondinone, B.M.; Boccuni, F.; Riccardo, F.; Bella, A.; Poletti, P.; Trentini, F.; Pezzotti, P.; Brusaferro, S.; et al. Retrospective analysis of the Italian exit strategy from COVID-19 lockdown. *Proc. Natl. Acad. Sci. USA* **2021**, *118*, e2019617118. [CrossRef] [PubMed]
28. Giordano, G.; Colaneri, M.; Di Filippo, A.; Blanchini, F.; Bolzern, P.; De Nicolao, G.; Sacchi, P.; Colaneri, P.; Bruno, R. Modeling vaccination rollouts, SARS-CoV-2 variants and the requirement for non-pharmaceutical interventions in Italy. *Nat. Med.* **2021**, *27*, 993–998. [CrossRef] [PubMed]
29. Mossong, J.; Hens, N.; Jit, M.; Beutels, P.; Auranen, K.; Mikolajczyk, R.; Massari, M.; Salmaso, S.; Tomba, G.S.; Wallinga, J.; et al. Social contacts and mixing patterns relevant to the spread of infectious diseases. *PLoS Med.* **2008**, *5*, e74. [CrossRef]
30. Giordano, G.; Blanchini, F.; Bruno, R.; Colaneri, P.; Di Filippo, A.; Di Matteo, A.; Colaneri, M. Modelling the COVID-19 epidemic and implementation of population-wide interventions in Italy. *Nat. Med.* **2020**, *26*, 855–860. [CrossRef]
31. Chinazzi, M.; Davis, J.T.; Ajelli, M.; Gioannini, C.; Litvinova, M.; Merler, S.; Pastore y Piontti, A.; Mu, K.; Rossi, L.; Sun, K.; et al. The effect of travel restrictions on the spread of the 2019 novel coronavirus (COVID-19) outbreak. *Science* **2020**, *368*, 395–400. [CrossRef] [PubMed]
32. Brauer, F.; Van den Driessche, P.; Wu, J.; Allen, L. *Mathematical Epidemiology*; Springer: Berlin/Heidelberg, Germany, 2008; Volume 1945.
33. Ziarelli, G.; Dede', L.; Parolini, N.; Verani, M.; Quarteroni, A. Optimized numerical solutions of SIRDVW multiage model controlling SARS-CoV-2 vaccine roll out: An application to the Italian scenario. *Infect. Dis. Model.* **2023**, *8*, 672–703. [CrossRef] [PubMed]
34. Shapiro, J.; Dean, N.; Madewell, Z.; Yang, Y.; Halloran, M.; Longini, I. Efficacy estimates for various COVID-19 vaccines: What we know from the literature and reports. *medRxiv* **2021**. [CrossRef]

35. Poletti, P.; Tirani, M.; Cereda, D.; Trentini, F.; Guzzetta, G.; Marziano, V.; Buoro, S.; Riboli, S.; Crottogini, L.; Piccarreta, R.; et al. Age-specific SARS-CoV-2 infection fatality ratio and associated risk factors, Italy, February to April 2020. *Eurosurveillance* **2020**, *25*, 2001383. [CrossRef] [PubMed]
36. Brazeau, N.; Verity, R.; Jenks, S.; Fu, H.; Whittaker, C.; Winskill, P.; Dorigatti, I.; Walker, P.; Riley, S.; Schnekenberg, R.P.; et al. *COVID-19 Infection Fatality Ratio: Estimates from Seroprevalence*; Report 34; Imperial College: London, UK, 2020.
37. Zhou, F.; Yu, T.; Du, R.; Fan, G.; Liu, Y.; Liu, Z.; Xiang, J.; Wang, Y.; Song, B.; Gu, X.; et al. Clinical course and risk factors for mortality of adult inpatients with COVID-19 in Wuhan, China: A retrospective cohort study. *Lancet* **2020**, *395*, 1054–1062. [CrossRef]
38. Del Valle, S.Y.; Hyman, J.M.; Chitnis, N. Mathematical models of contact patterns between age groups for predicting the spread of infectious diseases. *Math. Biosci. Eng. MBE* **2013**, *10*, 1475–1497.
39. Presidenza del Consiglio dei Ministri, Comitato Tecnico Scientifico. Report n°57 28 April 2020. Available online: https://emergenze.protezionecivile.gov.it/it/sanitarie/coronavirus/verbali-comitato-tecnico-scientifico/ (accessed on 1 February 2025).
40. Zhang, J.; Litvinova, M.; Liang, Y.; Wang, Y.; Wang, W.; Zhao, S.; Wu, Q.; Merler, S.; Viboud, C.; Vespignani, A.; et al. Changes in contact patterns shape the dynamics of the COVID-19 outbreak in China. *Science* **2020**, *368*, 1481–1486. [CrossRef] [PubMed]
41. Emanuel, E.; Philips, J.; Popescu, S. COVID-19 Activity Risk Levels July 2020. Available online: https://vitoli.ca/wp-content/uploads/2020/08/COVID-19-Risk-Index-Infographic-w-Authors-7.8.20-1.pdf (accessed on 1 February 2025).
42. Summan, A.; Nandi, A. Timing of non-pharmaceutical interventions to mitigate COVID-19 transmission and their effects on mobility: A cross-country analysis. *Eur. J. Health Econ.* **2022**, *23*, 105–117. [CrossRef]
43. Istituto Superiore di Sanità. *Epidemia COVID-19*; Aggiornamento Nazionale 10 Novembre 2021; Istituto Superiore di Sanità: Rome, Italy, November 2021.

Disclaimer/Publisher's Note: The statements, opinions and data contained in all publications are solely those of the individual author(s) and contributor(s) and not of MDPI and/or the editor(s). MDPI and/or the editor(s) disclaim responsibility for any injury to people or property resulting from any ideas, methods, instructions or products referred to in the content.